Say NO to Optimization: A Nonorthogonal Quantum Eigensolver

Unpil Baek,[1,2,3,*] Diptarka Hait,[4,5] James Shee,[4,†] Oskar Leimkuhler,[2,4,3] William J. Huggins,[4,§] Torin F. Stetina,[6,2] Martin Head-Gordon,[4,5,3] and K. Birgitta Whaley[4,2,3,‡]

[1] *Department of Physics, University of California, Berkeley, California 94720-7300, USA*
[2] *Berkeley Quantum Information and Computation Center, University of California, Berkeley, California 94720, USA*
[3] *Challenge Institute for Quantum Computation, University of California, Berkeley, California 94720, USA*
[4] *Department of Chemistry, University of California, Berkeley, California 94720-1460, USA*
[5] *Chemical Sciences Division, Lawrence Berkeley National Laboratory, Berkeley, California 94720, USA*
[6] *Simons Institute for the Theory of Computing, Berkeley, California 94704, USA*

(Received 26 May 2022; revised 21 April 2023; accepted 23 May 2023; published 17 July 2023)

A balanced description of both static and dynamic correlations in electronic systems with nearly degenerate low-lying states presents a challenge for multiconfigurational methods on classical computers. We present here a quantum algorithm utilizing the action of correlating cluster operators to provide high-quality wave-function ansätze employing a nonorthogonal multireference basis that captures a significant portion of the exact wave function in a highly compact manner and that allows computation of the resulting energies and wave functions at polynomial cost with a quantum computer. This enables a significant improvement over the corresponding classical nonorthogonal solver, which incurs an exponential cost when evaluating off-diagonal matrix elements between the ansatz states and is therefore intractable. We implement the nonorthogonal quantum eigensolver (NOQE) here with an efficient ansatz parametrization inspired by classical quantum chemistry methods that succeed in capturing significant amounts of electronic correlation accurately. Crucially, we avoid the need to perform any optimization of the ansatz on the quantum device. By taking advantage of such classical approaches, NOQE provides a flexible, compact, and rigorous description of both static and dynamic electronic correlation, making it an attractive method for the calculation of electronic states of a wide range of molecular systems.

DOI: 10.1103/PRXQuantum.4.030307

I. INTRODUCTION

The computation of electronic states and energies for molecular and extended systems, known as "the electronic structure problem," has emerged as one of the most prominent practical problems for which quantum computers might show an advantage over their classical counterparts. The worst-case quantum complexity of the electronic structure problem is known to be quantum Merlin-Arthur (QMA) complete [1], i.e., the quantum analog of NP hard. Although this implies that solving the general electronic structure problem to arbitrary accuracy may be intractable for quantum computers, a significant advantage over existing classical methods for systems of interest may still be achievable.

Focusing on molecular electronic systems, often referred to as "quantum chemistry," there are several facts that make the search for quantum algorithms in this area both interesting and suggestive of promise for demonstrating a quantum advantage. First, the level of accuracy required to make quantitative chemical predictions is 1 kcal/mol (approximately 1.6 mHa = 43 meV) or less (which corresponds to the reported uncertainties of typical experimental measurements for thermochemistry). This quantity is referred to as "chemical accuracy" [2]. Therefore, achieving arbitrary accuracy is not necessary for this high-impact domain-specific application of quantum algorithms. Second, energy splittings and relative orderings, which involve low-lying excited states in addition to the ground state, are of paramount importance in many problems of interest. This is especially true in so-called

*baek.un@berkeley.edu
†jshee@berkeley.edu
‡whaley@berkeley.edu
§current address: Google Quantum AI, San Francisco, CA 90291, USA.

"strongly correlated" electronic systems [3,4], wherein multiple spin states or phases are separated by small energy gaps. Such states can only be described by multiconfigurational wave functions composed of many Slater determinants, and chemically accurate *ab initio* predictions remain a challenge for existing classical computational methods.

A proper description of strong electronic correlation is required to describe a wide range of interesting physical phenomena, ranging from materials such as cuprates, which can exhibit long-range order and high-temperature superconductivity [5], to bond-breaking chemical reactions and the intricate electronic processes found in many biological and synthetic catalysts that contain magnetically coupled transition metals [6] or f-block atoms [7]. One very well-known system with multiple spin states is the oxygen-evolving complex (OEC) of photosystem II in green plants, which plays a critical role in the oxidation or "splitting" of water molecules to generate protons and free molecular oxygen [8]. This complex has four manganese atoms in different oxidation states [9], which are involved in a complex series of electron-transfer reactions that catalyze the oxidation of water [10]. Understanding the mechanism of this critical step in photosynthesis of green plants requires that the spin states involving the transition-metal atoms and the electronic states of coordinated reactants be well characterized, which presents a major challenge for quantum chemistry today. Efforts to perform electronic structure calculations with quantum computers started with an application of the quantum phase estimation (QPE) algorithm [11] that requires fault-tolerant quantum hardware and later shifted to approaches amenable to noisy intermediate-scale quantum (NISQ) hardware. These include a recently developed algorithm to solve a contracted Schrödinger equation for the two-particle reduced density matrix, from which associated energies can be obtained [12–14]. A more widely used hybrid quantum-classical algorithm is the variational quantum eigensolver (VQE) [15,16], in which the quantum computer is used to generate a wave-function ansatz with a parametrized quantum circuit, the expected value of the Hamiltonian terms are measured with this circuit, and the variational parameters are then optimized by a classical solver in an iterative manner [16]. By avoiding the large circuit depth necessary for QPE, approaches such as the VQE are more suitable for running on NISQ hardware.

Considerable efforts have gone into developing a broad range of different quantum circuit ansätze that approximate the ground states of Hamiltonians. The unitary coupled-cluster (UCC) ansatz, a unitary generalization of the coupled-cluster ansatz used in quantum chemistry, has been popular due to its variational and size-consistent nature [15–17]. However, the generic UCC ansatz requires a circuit depth that increases as higher-order terms in the coupled-cluster expansion are included, rendering hybrid calculations on near-term machines very sensitive to noise and limited by current constraints on qubit coherence. Furthermore, the classical optimization loop often requires many circuit evaluations even in the simplest cases [18,19]. The optimization problem is highly nonlinear and finding the global minimum can be challenging in practice [20]. This is complicated by the emergence of the "barren-plateau" phenomenon in many cases of interest, where randomness in the initial parameters, entanglement, or noise in the circuit leads to gradients that vanish exponentially with one or more problem parameters [21–25]. Hence there are two generic limitations of the VQE: (i) the qubits must have coherence times long enough to generate ansatz states with complex structures and (ii) the required number of measurements should not exceed the wall-clock time available for the near-term devices with consistent calibration.

An extension of the VQE has recently been proposed by some of the authors to allow greater expressivity of the final wave function without increasing the circuit depth [26]. This is the nonorthogonal VQE (termed NOVQE) that uses the quantum computer to generate a set of nonorthogonal ansatz states, on which the Hamiltonian and overlap matrices are measured using a modified Hadamard test. The resulting generalized eigenvalue problem is solved classically to provide an estimate of the ground-state energy, which is then optimized with respect to the circuit parameters for the set of nonorthogonal ansatz states. Results from the NOVQE in Ref. [26] have demonstrated a systematic increase in wave-function complexity and a greater fidelity with the true ground state, relative to that obtained with the VQE using a single-reference-state ansatz. But this comes at the cost of a greater number of measurements. Therefore, the NOVQE presents a trade-off between decreased requirements on qubit coherence time for an increased number of circuit repetitions and, consequently, also an increase in the measurement cost.

To break out of this inevitable trade-off for variational hybrid quantum algorithms, we present here a novel quantum algorithmic approach to electronic structure calculations that does not use variational optimization. The nonorthogonal quantum eigensolver proposed in the current work, which we refer to as NOQE, takes advantage of domain-specific knowledge available in classical quantum chemistry to construct high-quality wave functions at a low cost. Specifically, our protocol uses spin-unrestricted methods that optimize spin-symmetry-broken Slater determinants (i.e., with different spatial distributions for the up and down spins) to yield more accurate energies and electronic densities in the strongly correlated limit. Explicit diagonalization within the subspace spanned by all qualitatively relevant unrestricted single determinants, known in the classical quantum chemical literature as nonorthogonal configuration interaction or NOCI, offers a straightforward way to approximate spin purification of unrestricted solutions [27–29]. However, while strong correlations are

reasonably well addressed by the classical NOCI approach [29,30], taken alone this protocol cannot recover the weak (dynamical) correlation present in the system. In the current work, we show that the effects of dynamical correlation can be introduced via the application of UCC-like operators to the subspace states with perturbative parameters. This "perturb and then diagonalize" approach confers the advantage of computing at once both the ground and low-lying excited states of the system through subspace diagonalization, with approximately correct spin quantum numbers. Consequently, the energy gaps between the different low-lying spin states of a strongly correlated electronic system can be easily computed. The application of UCC-like operators can be efficiently implemented on quantum computers. Furthermore, by making a subspace diagonalization on the resulting states, NOQE also avoids the long-time evolution (and consequent deep circuits) required by other optimization-free hybrid quantum algorithms [31–35].

The quantum computational advantage of the NOQE approach comes from the efficient calculation of off-diagonal matrix elements on a quantum computer. Classical evaluation of a single NOCI matrix off-diagonal element has only $\mathcal{O}(N^2)$ asymptotic cost with the basis size N. However, the inclusion of dynamic correlation with CC operators (perturbative or otherwise) results in each off-diagonal element having a classical cost that scales $\mathcal{O}(\exp(N))$. On the other hand, evaluation of these matrix elements via the modified Hadamard test of Ref. [26] scales with $\mathcal{O}(\text{poly}(N))$. In principle, this allows for an exponential separation between quantum and classical nonorthogonal quantum chemistry calculations. In this work, we explore the quality of the NOQE approach using both a UCC-derived ansatz and a cluster-Jastrow (CJ) modification thereof. We make a resource estimate for NOQE with these ansätze and give a prognosis for the extent to which classically intractable NOCI calculations including dynamic correlation may be efficiently realized by our quantum NOQE approach.

The remainder of the paper is structured as follows. In Sec. II, we discuss the background of current classical quantum chemistry methods available for electronic structure calculations for systems with strong correlation. In Sec. III, we introduce the NOQE protocol after presenting an essential preliminary analysis of the modified UCC wave-function ansätze used in this work. In Sec. IV, we present numerical results for two simple model systems accessible on near-term devices—the potential-energy surfaces of molecular hydrogen H_2 and square H_4—which nevertheless exhibit regimes of strong static correlation that are challenging for traditional single-reference methods (see below). For this reason, stretched H_2 and square H_4 are frequently used to assess new electronic structure methods for strongly correlated systems [20,26]. In Sec. V, we analyze the scaling of quantum circuit resources needed to run the NOQE routine on a quantum computer for molecular systems. Finally, in Sec. VII, we summarize and provide an outlook for both theoretical and experimental developments suggested by this work.

II. BACKGROUND

Quantum chemistry aims to develop computationally affordable approximations for modeling the quantum many-body problem. The simplest quantum chemistry method is the Hartree-Fock (HF) approximation [36], which provides a mean-field description of the many-electron ground-state wave function by variationally optimizing a single Slater determinant (an antisymmetrized product of single-particle orbitals [36]). The computational cost of Hartree-Fock calculations scales as $\mathcal{O}(N^4)$. While global minimization of the Hartree-Fock procedure is formally an NP-complete problem [37], in most cases the physically motivated heuristics involved in Hartree-Fock calculations nevertheless allow for efficient convergence to local minima. The energy not captured by this independent-particle approximation is typically referred to as the electron correlation energy, which is often broadly categorized into "weak (dynamic)" and "strong (static)" (although no rigorous boundary exists between the two limits).

Nevertheless, a distinction between weak and strong correlations can be made in terms of limiting behavior. The Hartree-Fock approximation works best when the true wave function is well approximated by a single Slater determinant, wherein the orbitals are filled in ascending order of energy and are doubly occupied (with one spin-up electron and one spin-down electron) when possible. However, the strong correlation between electrons makes it energetically unfavorable to maintain electron pairs, leading to a (partial) separation of paired electrons into distinct orbitals occupying different spatial regions. Strong correlation, therefore, entails a significant level of electron-pair breaking, which requires several Slater determinants to have significant weights in the wave function. On the other hand, weak electron correlation does not require electron unpairing and largely stems from small but significant contributions of many electronic configurations with individually small amplitudes in the overall wave function. Traditional quantum chemistry has been quite successful at modeling weak correlation for systems where the Hartree-Fock approximation is qualitatively valid ("single-reference"), through perturbative [38] and projected coupled-cluster [39] approaches that have only polynomial scaling with N. Systems with strong correlation are more challenging and generally require solving the exact diagonalization or full CI (FCI) problem within some subspace of orbitals [40]. This has an exponential cost and exact treatment is only feasible for small subspaces up to 24 spatial orbitals [41] at present (selected CI solvers

permit substantially larger orbital spaces with soft exponential scaling [42–45]). In addition, weak correlation outside the subspace is essential for chemical accuracy [46–48] and can add considerably to the computational cost.

One possible route to describing strong correlations starting from mean-field theory is via spin-symmetry breaking. It is possible to converge Slater determinants where the up and down spin orbitals have different spatial components and can thus accommodate a level of electron unpairing. The down side of such spin-unrestricted Hartree-Fock calculations is that the resulting determinant is no longer a pure spin eigenstate and therefore cannot be used to estimate the spin spectrum. Restoration of spin symmetry is also quite challenging for single-reference wave-function methods, often leading to suboptimal performance of such approaches utilizing an unrestricted reference [49]. However, unrestricted determinants have much better energies and total electron densities [36], making them attractive candidates for modeling strongly correlated systems if spin purity can be realized.

Classically, the NOCI approach offers a reasonably straightforward route to an approximate spin purification of such unrestricted solutions [29]. Explicit diagonalization within the subspace spanned by all unrestricted configurations corresponding to different permutations of all (partially or completely) unpaired spins should therefore lead to pure spin states, via indirectly coupling the angular momenta. In practice, the resulting states are not always quite pure in spin, due to differences in orbitals corresponding to stationary states for each permuted configuration. However, they are much better approximations to spin eigenstates than are the untreated unrestricted single determinants and, furthermore, they also permit computation of spin-gap energies.

Compared with multideterminant expansions that use a single shared set of orbitals, NOCI can describe multireference states with a more compact linear combination of determinants. The physical intuition behind this can be illustrated by the dissociation of NaCl (a similar argument holds for H_2). In the region of the avoided crossing, there is a competition or mixing between the covalent and ionic diabatic states. If forced to use only a single set of orbitals, both the covalent and ionic configurations will be suboptimally described. In contrast, NOCI allows each configuration to have optimized orbitals, such that, for example, the large electron-density rearrangement going from covalent to ionic configurations can be efficiently represented (orbital expansion on Cl^- relative to Cl; orbital contraction on Na^+ relative to Na). The ability of NOCI to efficiently describe such configuration-specific orbital-relaxation effects provides similar advantages for many polynuclear transition-metal compounds, where the electron and hole densities of bridging or ligand moieties have the flexibility to optimally rearrange for each electron configuration involving the metal centers.

In practice, however, NOCI with single determinants is not very accurate, because the CI protocol only recovers the strong correlation between the unpaired electrons [29,30,50]. Weak correlation can be included via a "perturb and then diagonalize" approach, in which NOCI is performed within a subspace of unrestricted wave functions that already include a measure of dynamic correlation. NOCI using unitary coupled-cluster (UCC) wave functions, where the UCC states are constructed from unrestricted Hartree-Fock solutions, falls into the latter category and this is the route that we explore in this work. However, for classical computers, the computational demands of UCC amplitude optimization are considerable, particularly for nonorthogonal problems. It is important to note that the classical cost of computing the UCC operator for a single-reference determinant scales exponentially with the number of spin orbitals. For this reason, the projected coupled-cluster approaches [39] widely used in classical quantum chemistry do not evaluate energies as the expectation value of the Hamiltonian over the full coupled-cluster wave function, since that task also has an exponential classical cost. Instead, a formally nonvariational single-reference energy is defined via projection equations that can be solved at an increasing high-scaling polynomial cost as more correlations are included in the CC operator [51]. For example, the commonly used CCSD approach (single and double excitations from a Hartree-Fock reference state) scales as $\mathcal{O}(N^6)$ and the CCSDT approach (single, double, and triple excitations) scales as $\mathcal{O}(N^8)$, and so on (so-called local correlation approximations can reduce this scaling at the expense of some numerical error [52–54]). However, this classical approach does not readily generalize to off-diagonal matrix elements between multiple coupled-cluster states. Indeed, any use of coupled-cluster wave functions for direct evaluation of off-diagonal elements would incur an exponential cost for even orthogonal reference states. The situation is even more challenging for the nonorthogonal case because the Slater-Condon rules [36] cannot be applied to simplify many terms to zero, incurring an even higher cost. Therefore, the advantage of using a quantum processor in NOQE is not only due to the simple implementation of the UCC operator within a quantum algorithm for generating the reference states of a NOCI problem but also because the standard projected coupled-cluster theory is computationally intractable for the NOCI problem on classical computers. This provides strong motivation for the introduction of NOQE in this work as a quantum algorithm yielding a substantial quantum advantage relative to NOCI.

In this work, we therefore explore the use of amplitudes derived from the perturbative analysis in NOQE calculations without further optimization. This is expected to be a reasonable assumption because the amplitudes from second-order many-body perturbation theory (known as

MP2) are first-order approximations to actual UCC amplitudes, as is shown explicitly in Sec. III B 1. We denote this version of NOQE using UCC ansätze, together with MP2 amplitudes, as NOUCC(2). We note that NOUCC(2) ground-state energies are variational in the sense that they are bounded from below by the exact FCI energy, which provides a lower bound on diagonalization of the Hamiltonian within a NO subspace of wave functions. As an alternative, we also examine the benefits of adding a CJ correlator to a UCC ansatz, i.e., using the UCJ ansatz of Ref. [55]. We denote the version of NOQE using this ansatz as the NOUCJ.

III. THEORY

We first define the notation employed in this work and then provide, in Sec. III B, some preliminary analysis for the construction of the NOUCC(2) ansatz reference states, as well as the alternative NOUCJ ansatz based on a CJ decomposition. The general NOQE approach is then presented in Sec. III C, together with details of the quantum circuit implementation.

A. Notation

We define N as the number of spin orbitals and make use of the Jordan-Wigner transformation to map electronic states (determinantal wave functions) constructed from these to a qubit representation [56]. Then, N is the number of qubits required to represent the quantum state. We use η to represent the number of electrons and r to denote the number of radical sites (the number of active fractionally occupied orbitals relevant to the static correlation) involved in a specific molecular calculation (Sec. V). All references to orbitals in this work are to molecular orbitals (MOs) unless specified otherwise; the MOs are assumed to be real. The MOs are generally expressed as linear combinations of Gaussian basis functions in quantum chemistry, for ease of computation. Indices $\{i,j\}$ refer to occupied spin orbitals, indices $\{a,b\}$ to virtual spin orbitals, and indices $\{p,q,r,s\ldots\}$ are employed to represent general spin orbitals. Capitalized indices $\{I,J\}$ are used to index the reference states for the generalized eigenvalue equation of NOQE, with a total number of M reference states (determinants). We follow the chemistry convention that spin-up electrons are referred to as α electrons and spin-down electrons as β electrons.

The two-electron repulsion integrals (ERIs) between MOs are abbreviated according to standard chemical notation as

$$\langle ij\,|ab\rangle = \int d\vec{r} \int d\vec{r}\,' \frac{\phi_i(\vec{r})\,\phi_j(\vec{r}\,')\,\phi_a(\vec{r})\,\phi_b(\vec{r}\,')}{|\vec{r}-\vec{r}\,'|}, \quad (1)$$

$$\langle ij\,||ab\rangle = \langle ij\,|ab\rangle - \langle ij\,|ba\rangle. \quad (2)$$

The unitary coupled-cluster doubles (UCCD) ansatz is defined, in this work, relative to a Hartree-Fock reference state $|\Phi_{\mathrm{HF}}\rangle$ as $e^{\hat{\tau}}|\Phi_{\mathrm{HF}}\rangle$, with

$$\hat{\tau} \equiv \hat{T} - \hat{T}^{\dagger}, \quad (3)$$

$$\hat{T} = \sum_{pqrs=1}^{N} t_{ps,qr}\hat{a}_p^{\dagger}\hat{a}_q^{\dagger}\hat{a}_r\hat{a}_s \quad (4)$$

$$= \sum_{pqrs=1}^{N} t_{ps,qr}\hat{a}_p^{\dagger}\hat{a}_s\hat{a}_q^{\dagger}\hat{a}_r, \quad (5)$$

where the $N^2 \times N^2$ supermatrix $\mathbf{T}$ is defined by its grouped two-index matrix elements

$$t_{ps,qr} \equiv \begin{cases} t_{pqrs}, & p<q; s<r; r,s \in \mathrm{occ}; p,q \in \mathrm{virt}, \\ 0, & \text{otherwise.} \end{cases} \quad (6)$$

In the above, the four-index t_{pqrs} refer to the standard UCCD amplitudes. The primary focus of the present work is the use of MP2 amplitudes for t_{pqrs} (generating the NOUCC(2) ansatz), which we denote as t_{pqrs}^{MP2}. However, we also consider the use of Jastrow-correlated amplitudes (generating the NOUCJ ansatz), which we denote as t_{pqrs}^{J}. We refer to the cluster operator with MP2 amplitudes as UCC-MP2 and to the cluster operator with Jastrow-correlated amplitudes as UCC-J.

B. Preliminaries

1. MP2 amplitudes as first-order approximation to UCCD amplitudes

Here, we derive a first-order approximation to the UCCD amplitudes t_{abij} in terms of MP2 amplitudes obtained from perturbation theory. Suppose that we have a UCC wave function given by

$$\left|\Psi(\{t_{abij}\})\right\rangle = e^{\hat{\tau}}\,|\Phi_{\mathrm{HF}}\rangle\,, \quad (7)$$

with $\hat{\tau}$ given by Eqs. (5) and (6). We approximate the amplitudes $\{t_{abij}\}$ via gradient descent in the space of t amplitudes. For example, starting from the case where all $t_{abij} = 0$, the gradient of the energy with respect to t_{abij} is

$$\left(\frac{\partial E}{\partial t_{abij}}\right)_{\{t_{abij}\}=0} = \langle\Phi_{\mathrm{HF}}|\,[\hat{H}, \hat{a}_a^{\dagger}\hat{a}_b^{\dagger}\hat{a}_j\hat{a}_i]\,|\Phi_{\mathrm{HF}}\rangle \quad (8)$$

$$= \langle ij\,||ab\rangle\,, \quad (9)$$

and the diagonal elements of the Hessian are readily evaluated as

$$\left(\frac{\partial^2 E}{\partial t_{abij}^2}\right)_{\{t_{abij}\}=0} = \langle\Phi_{\rm HF}|\left(\hat{a}_a^\dagger\hat{a}_b^\dagger\hat{a}_j\hat{a}_i\right)^\dagger \hat{H}\hat{a}_a^\dagger\hat{a}_b^\dagger\hat{a}_j\hat{a}_i|\Phi_{\rm HF}\rangle - \langle\Phi_{\rm HF}|\hat{H}|\Phi_{\rm HF}\rangle \quad (10)$$

$$\approx \epsilon_a + \epsilon_b - \epsilon_j - \epsilon_i, \quad (11)$$

where ϵ_i denotes the single-particle energy of orbital i. A first-order Newton-Raphson approximation to t_{abij} is then given by

$$t_{abij} = -\frac{\left(\frac{\partial E}{\partial t_{abij}}\right)_{\{t_{abij}\}=0}}{\left(\frac{\partial^2 E}{\partial t_{abij}^2}\right)_{\{t_{abij}\}=0}} \approx -\frac{\langle ij||ab\rangle}{\epsilon_a+\epsilon_b-\epsilon_j-\epsilon_i}, \quad (12)$$

which is seen to be identical to the t amplitudes that would be obtained from second-order perturbation theory, i.e., from MP2. In fact, the energy of the wave function $|\Psi(\{t_{abij}^{\rm MP2}\})\rangle$ is correct not only to the second order in MP perturbation theory but to the third. We also note that this protocol predicts zero single-excitation amplitudes from unrestricted Hartree-Fock reference determinants, consistent with Brillouin's theorem [36]. MP2 amplitudes have consequently been used to initialize VQE optimizations for UCCSD [57].

We note that using the exact form of Eq. (10) would lead to Epstein-Nesbet perturbation theory [58,59] instead, which is known to be inferior to MP2 for single Slater determinants [60] and is therefore not explored here. We do, however, note that there are some other routes to improve upon using bare MP2 $\{t_{abij}\}$. Perhaps the simplest route is via scaling t_{abij}, in the spirit of a line search. The scaling MP2 of parameters has precedence in classical quantum chemistry, with Ref. [61] proposing that empirically scaling the same-spin amplitudes (i.e., all of a, b, i, and j have the same spin) by 0.33 and opposite-spin amplitudes (i.e., i and j have different spin, and so do a and b) by 1.2 would lead to better results. Reference [62] has gone even further and has neglected same-spin amplitudes entirely, scaling opposite-spin amplitudes by 1.3. These spin-component-scaled (SCS) and scaled-opposite-spin (SOS) MP2 methods yield superior quantitative performance to normal MP2 [61,62], indicating that unscaled MP2 appears to underestimate opposite-spin correlation. Furthermore, the very slow convergence of MP theory for spin-contaminated systems [49] indicates the possibility of unscaled MP2 amplitudes being too small in the spin-polarized limit. Scaling up the amplitudes thus has the potential to be more effective. We therefore explore whether SCS- or SOS-style scalings affect the NOUCC(2) results and we also investigate whether uniform scaling of the amplitudes is effective.

2. *Single-reference-state generation: Quantum circuit ansatz based on the low-rank decomposition*

To simulate the action of the unitary cluster operator, we employ the technique of low-rank tensor decomposition [63,64], which has been previously introduced and utilized in classical contexts [65–67]. In this approach, we decompose the rank-4 doubles cluster tensor $\hat{\tau} = \hat{T} - \hat{T}^\dagger$ [Eqs. (3)–(5)] into a sum-of-squares of one-electron normal operators. This can be done using either a singular-value decomposition (SVD) or a Takagi factorization [63,64], to yield

$$e^{\hat{\tau}} = \exp\left(-i\sum_{l=1}^{L}\sum_{\mu=1}^{m}\hat{Y}_{l,\mu}^2\right), \quad (13)$$

where the number of nonzero singular values (or Takagi diagonals) $L \le N^2$ and $m = 4$ if the decomposition is by SVD or $m = 2$ if the Takagi factorization has been used (this may increase L by up to a factor of 2; see Sec. S2 of the Supplemental Material [68], which includes Refs. [69–79]). The (normal) operators $\hat{Y}_{l,\mu}$ are then further diagonalized and the resulting unitary is Trotterized to obtain the final low-rank form of the state-preparation ansatz as

$$e^{\hat{\tau}} \approx \hat{\mathcal{U}}_B^{(1,1)\dagger}\prod_{l=1}^{L}\prod_{\mu=1}^{m}\exp\left(-i\sum_{pq}^{\rho_l}\lambda_p^{(l,\mu)}\lambda_q^{(l,\mu)}\hat{n}_p\hat{n}_q\right)\tilde{\mathcal{U}}_B^{(l,\mu)}. \quad (14)$$

Here, $\lambda_p^{(l,\mu)}$ are eigenvalues of the $\hat{Y}_{l,\mu}$ operators and the total number of nonzero eigenvalues is $\rho_l \le N$. The unitary operators $\hat{\mathcal{U}}_B^{(1,1)\dagger}$ are single basis rotations and $\tilde{\mathcal{U}}_B^{(l,\mu)}$ are sequences of neighboring basis rotations (see Sec. S2 of the Supplemental Material [68]). The approximation in the above decomposition is entirely due to Trotter error. The effect of this error on the energy-expectation values can be made arbitrarily small by increasing the order of the Trotter expansion (see Sec. S4 of the Supplemental Material [68]).

The double decomposition of Eq. (14) results in a circuit structure of blocks of alternating unitary basis rotations ($\tilde{\mathcal{U}}_B^{(l,\mu)}$) requiring up to $2\binom{N/2}{2}$ nearest-neighbor Givens rotations [63,80] and sets of exponentiated number-operator pairs that require at most $\binom{N}{2}$ two-qubit controlled-Z (CZ) gates on a fully connected architecture, which may be applied in N layers of parallel gates [63] (for further details of the resource estimation, see Sec. V). We note that one-body excitation terms can easily be included in the ansatz, requiring only an additional single basis rotation in front of the product in Eq. (14) and resulting in an additional cost of up to $2\binom{N/2}{2}$ Givens rotations.

The representation in Eq. (14) is advantageous for two reasons. First, the low-rank decomposition allows us to systematically truncate the rank of the MP2 $\hat{\tau}$-tensor by thresholding the singular values, reducing the number of circuit blocks and hence the overall circuit depth, while preserving the desired level of accuracy in the ansatz. Second, the Jordan-Wigner mapping from orbitals to qubits requires lengthy strings of Z gates to encode fermionic anticommutation relations in excitations ($\hat{a}_p^\dagger \hat{a}_q$) between geometrically distant qubits p and q, which results in multiple additional layers of controlled-NOT (CNOT) gates per excitation term [81,82]. By rotating into bases where the fermionic excitations are represented by number operators ($\hat{n}_p = \hat{a}_p^\dagger \hat{a}_p$), these Jordan-Wigner strings are entirely avoided, significantly reducing the circuit depth.

3. Single-reference-state generation: adding Cluster-Jastrow correlators

In this work, we also explore the addition of Jastrow correlations to the MP2 approximation to the UCCD ansatz wave functions, leading to the NOUCJ modification of NOQE. We show below that incorporating Jastrow correlations allows for a more expressive but equally compact representation, suggesting that this approach is compatible with a lower truncation of the tensor decomposition and showing potential for implementation with shorter quantum circuits than the NOUCC(2) reference ansatz.

The idea of applying a two-or-more-electron Jastrow correlator to a Slater determinant, i.e., $e^{\hat{J}}|\phi\rangle$, has first been introduced to efficiently satisfy the well-known cusp condition [83] and forms the basis of classical quantum chemistry methods such as variational and diffusion Monte Carlo [84,85]. In such methods, the Jastrow term is typically represented in real space, although Neuscamman and others have recently developed promising approaches in which a CJ correlator in orbital space appears in front of the antisymmetrized geminal power (pairing) ansatz [86–88]. A unitary variant of the CJ operator, denoted UCJ, has recently been proposed in Ref. [55], where the cluster operator takes the form

$$e^{\hat{\tau}} = \prod_{l=0}^{L} e^{\hat{\mathcal{K}}_l} e^{\hat{\mathcal{J}}_l} e^{\hat{\mathcal{K}}_l}, \tag{15}$$

with $\hat{\mathcal{K}}_l = \sum_{pq} \mathcal{K}^l_{pq} \hat{a}_p^\dagger \hat{a}_q$ and $\hat{J}_l = \sum_{pq} \mathcal{J}^l_{pq} \hat{n}_p \hat{n}_q$. The $\boldsymbol{\mathcal{K}}$ matrices are complex and anti-Hermitian, while the $\boldsymbol{\mathcal{J}}$ matrices are symmetric and purely imaginary. As a result, the (generally complex) amplitudes of the UCCD operator can then be represented as

$$t^J_{pqrs} = \sum_l \sum_{jk} U^l_{pj} U^{l,*}_{qj} \mathcal{J}^l_{jk} U^l_{rk} U^{l,*}_{sk}, \tag{16}$$

where the unitaries $\hat{U}$ are the basis-rotation operators. As noted in Ref. [55], this form is identical to the double-SVD decomposition shown in Eq. (14) when $\lambda_i \lambda_j \to \mathcal{J}_{ij}$. As such, the UCJ ansatz has the potential to be slightly more expressive. We note also that while the unitaries and λ eigenvalues that result from double factorization are determined by the cluster amplitudes (which for NOUCC(2) are taken from a classical MP2 calculation), in the UCJ ansatz [cf. Eq. (15)] the matrix elements of $\boldsymbol{\mathcal{K}}$ and $\boldsymbol{\mathcal{J}}$ are classically optimized variationally. Furthermore, it has been demonstrated that significantly fewer l terms are required to recover high accuracy comparable to exact results [55], thereby providing a promising avenue toward reduced-depth quantum circuits.

In this work, we illustrate the use of the UCJ ansatz with $L = 1$ in a NOQE calculation, denoted NOUCJ($L = 1$), for the H_2 system in the STO-3G basis. Accuracy comparable to that of untruncated (i.e., $L = N^2$) NOUCC(2) is achieved, suggesting that variational optimization of the Jastrow ansatz parameters can effectively compensate for the relatively small number of these imposed by truncation. We note that by construction, the $L = 1$ UCJ ansatz does not require further Trotterization, which is not the case for doubly factorized reference ansätze in the NOUCC(2) procedure.

C. Nonorthogonal quantum eigensolver (NOQE)

We now come to the main theoretical exposition of this work, which is the construction of a NOQE that does not require variational optimization. We construct multireference ansatz state as a linear combination of M UHF base reference states:

$$\left|\Psi_{\mathrm{NOUCC(2)}}\right\rangle = \sum_{J=1}^{M} c_J \left|\phi_J\right\rangle = \sum_{J=1}^{M} c_J e^{\hat{\tau}_J} \left|\Phi_J\right\rangle. \tag{17}$$

Here, $|\Phi_J\rangle$ and $\hat{\tau}_J$ are, respectively, the Jth UHF base reference state and the corresponding Jth two-body excitation MP2 tensor, which is constructed in the single-particle basis of $|\Phi_J\rangle$. Key features of this expansion, which also distinguish this work from the previous NOVQE work [26], are first that more than one base reference state is employed and, second, that the base reference states are unrestricted Hartree-Fock states rather than restricted Hartree-Fock state, i.e., UHF rather than RHF. Since all base reference states are described by their expansion in the underlying common atomic orbital basis, the first feature introduces the need to track the unitary transformations between these expansions (see Sec. S1C of the Supplemental Material [68]). The second feature introduces significantly greater flexibility for the description of strongly correlated systems.

The NOQE coefficients c_J are determined by classically diagonalizing the Hamiltonian matrix in the subspace of

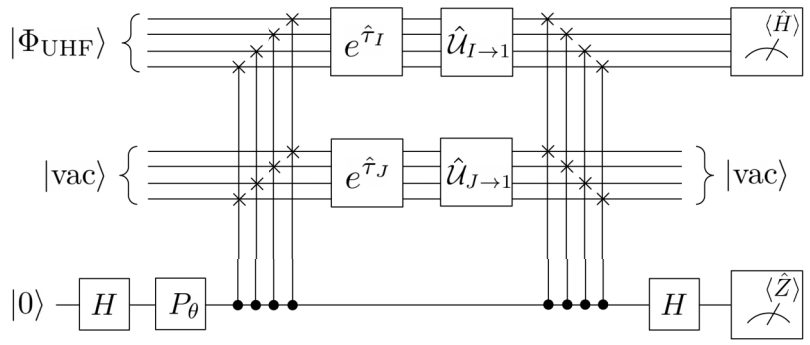

FIG. 1. The NOQE circuit for the evaluation of off-diagonal matrix elements of the Hamiltonian (H_{IJ}) and overlap matrix (S_{IJ}) between NOUCC(2) ansatz states $|\phi_I\rangle$ and $|\phi_J\rangle$. For the phase gate P_θ, we set $\theta = 0$ ($P_\theta = I$) when measuring $\mathrm{Re}(H_{IJ})$ and $\theta = \pi/2$ when measuring $\mathrm{Im}(H_{IJ})$ (see Sec. S3 of the Supplemental Material [68]).

these nonorthogonal reference states. This requires solving the generalized eigenvalue problem

$$\mathbf{H}\vec{c} = E\mathbf{S}\vec{c}, \tag{18}$$

with Hamiltonian and overlap matrix elements given by

$$H_{IJ} = \langle\phi_I|\,\hat{H}\,|\phi_J\rangle\,, \quad S_{IJ} = \langle\phi_I|\phi_J\rangle. \tag{19}$$

Provided that the **S** matrix is far from singular and therefore the solutions to Eq. (18) are numerically stable, this small eigenvalue problem is trivial for a classical computer. We note that even in the near-singular case, it can be solved reliably using the standard procedure of thresholding the singular values of **S** and the numerical analysis of this procedure has been carefully analyzed recently [89].

We evaluate the off-diagonal elements of the Hamiltonian and overlap matrices [Eq. (19)] using a quantum circuit that is closely related to the modified Hadamard test protocol of Ref. [26]. Figure 1 shows the general circuit for NOQE calculations using different NOUCC(2) ansatz states. The input to the circuit is an N-qubit reference state $|\Phi_{\mathrm{UHF}}\rangle$, an ancilla register of size N, and a single control qubit, resulting in a total of $2N + 1$ qubits. The η-electron UHF state in the first single-particle basis is prepared as $|\Phi_{\mathrm{UHF}}\rangle = |1\rangle^{\otimes\eta} \otimes |0\rangle^{\otimes N-\eta}$. For the example of H_2 in the STO-3G basis with four spin orbitals (see Table I), we would have $|\Phi_{\mathrm{UHF}}\rangle = |1100\rangle$. The operation of the circuit in Fig. 1 and its implementation of a modified Hadamard test for the evaluation of the off-diagonal Hamiltonian and overlap-matrix elements of Eq. (19) is described in detail in Sec. S3 of the Supplemental Material [68].

Note that in contrast to the circuit employed in the NOVQE of Ref. [26], which employs nonorthogonal reference states constructed with respect to a single (spin-restricted) Hartree-Fock state, the circuit of Fig. 1 contains additional unitaries that rotate the atomic orbital bases on each register from that of UHF reference I or J into the (arbitrarily chosen) first single-particle basis, i.e., $\hat{\mathcal{U}}_{J\to 1}$. This accounts for the fact that the NOQE reference states are constructed here over different UHF basis sets, while the computation of the matrix elements and overlaps requires a consistent mapping of the orbital space onto the qubit register for all of the reference states, as well as the system Hamiltonian. We apply the unitary basis rotation following the preparation of the ansatz state in the default basis of the quantum register, which is equivalent under cancelation of unitaries to the transformation

$$|\Phi_J\rangle \mapsto \hat{\mathcal{U}}_{J\to 1}\,|\Phi_{\mathrm{UHF}}\rangle\,, \tag{20}$$

$$e^{\hat{\tau}_J} \mapsto \hat{\mathcal{U}}_{J\to 1} e^{\hat{\tau}_J} \hat{\mathcal{U}}^\dagger_{J\to 1}. \tag{21}$$

Thus, on the right-hand side of Eqs. (20) and (21), $|\Phi_{\mathrm{UHF}}\rangle$ and $e^{\hat{\tau}_J}$ are implemented in the default basis but are implicitly understood to be representations in the Jth UHF basis, prior to the application of $\hat{\mathcal{U}}_{J\to 1}$, after which everything is correctly expressed in the same (first) UHF basis. The basis rotation is constructed in terms of the $N \times N$ coefficient matrices $\mathbf{C}_J$ transforming the atomic orbital basis to the Jth molecular orbital basis and the atomic orbital

TABLE I. The size resources required for evaluation of matrix elements of the Hamiltonian and overlap for H_2 and H_4 with different basis sets (for definition of these, see Sec. S1 of the Supplemental Material [68]). The last column shows the number of qubits required to construct the NOQE circuit of Fig. 1.

System	Basis set	Basis functions per H atom	Spin orbitals, N	Qubits, $2N$+1
H_2	STO-3G	1	4	9
	6-31G	2	8	17
	6-311G	3	12	25
H_4	STO-3G	1	8	17

overlap matrix $\mathbf{S}_A$:

$$\hat{\mathcal{U}}_{J\to 1} = \exp\left(\sum_{pq=1}^{N} [\ln(\mathbf{C}_J^T \mathbf{S}_A \mathbf{C}_1)]_{pq} (\hat{a}_p^\dagger \hat{a}_q - \hat{a}_q^\dagger \hat{a}_p)\right). \tag{22}$$

This can be efficiently implemented with Givens rotations and single-qubit rotation gates, even over a device with linear connectivity [80] (see Sec. V). We note that the circuit can be modified to reduce the gate cost by transforming one of the two reference ansatz states to the basis of the other one, rather than transforming both to the common basis $I = 1$. This modification is employed in obtaining the resource estimate counts in Sec. V.

While the current work focuses on ground and low-lying electronic energy states, we point out that one may also replace the UHF reference state in the circuit diagram of Fig. 1 with a UHF state representing an excited electronic configuration to find other higher-lying states. For example, the excited determinant $|\Phi_i^a\rangle$, where $i \le \eta$ and $a > \eta$, would be prepared by $X_i |1\rangle^{\otimes \eta} \otimes X_a |0\rangle^{\otimes N-\eta}$, where X_p denotes a bit-flip gate acting on the pth qubit.

One additional benefit of performing the measurements using the modified Hadamard test is that we can thereby directly incorporate the reduced overhead measurement techniques of Ref. [90] without increasing the circuit depth. The basic idea is to apply a tensor factorization to the two-body part of the Hamiltonian, similar to the one described for the cluster tensor in Eq. (14):

$$\hat{H} \approx \sum_{l=1}^{L} \hat{\mathcal{U}}_B^{l\dagger} \left(\sum_{pq} \lambda_p^{(l)} \lambda_q^{(l)} \hat{n}_p \hat{n}_q\right) \tilde{\mathcal{U}}_B^l. \tag{23}$$

One can then measure all of the $\hat{n}_p \hat{n}_q$ terms corresponding to a particular value of l simultaneously by explicitly applying the change of basis $\hat{\mathcal{U}}_B^l$ on the quantum device before performing a standard measurement in the computational basis. In our case, this can be accomplished without any additional quantum resources, because the product $\hat{\mathcal{U}}_B^l \hat{\mathcal{U}}_{J\to 1}$ amounts to a single change of basis and can be implemented using the same number of gates as $\hat{\mathcal{U}}_{J\to 1}$ alone. Empirically, it has been found that taking $L = \mathcal{O}(N)$ is sufficient to obtain a fixed relative error in the energy due to the decay of the singular values in the first tensor factorization of the Hamiltonian [66]. Reference [90] has found that taking advantage of the decomposition in Eq. (23) reduces the variance of the energy estimator by orders of magnitude, even for small VQE calculations. More study in the context of the off-diagonal matrix-element measurements considered here will be useful.

There are also variants of the NOQE circuit that can reduce the number of qubits required from $2N + 1$ to $N + 1$. In this case, however, the circuit depth will need to be approximately doubled to accommodate application of all four unitaries $e^{\hat{\tau}_I}$, $\hat{\mathcal{U}}_{I\to 1}$, $\hat{\mathcal{U}}_{J\to 1}^\dagger$, and $e^{-\hat{\tau}_J}$ to the N system qubits. Suppose that the Hamiltonian (expressed in the first UHF basis) is decomposed as a linear combination of Pauli operators, $\hat{H} = \sum_k c_k \hat{P}_k$. One strategy for reducing the number of qubits would then be to use a single-ancilla qubit to perform a Hadamard test on each of the unitary operators $e^{-\hat{\tau}_J} \hat{\mathcal{U}}_{J\to 1}^\dagger \hat{P}_k \hat{\mathcal{U}}_{I\to 1} e^{\hat{\tau}_I}$, estimating their expectation values with respect to $|\Phi_{\mathrm{UHF}}\rangle$. Naively, this requires us to condition the application of the state-preparation unitaries on the state of the ancilla qubit.

However, as with the generic case of Fig. 1 in which $2N + 1$ qubits are used, we can take advantage of the fact that the state-preparation unitaries conserve particle number. Rather than explicitly conditioning them on the state of the ancilla qubit, we can instead use the ancilla to control the preparation and uncomputation of $|\Phi_{\mathrm{UHF}}\rangle$ from the vacuum state, together with the operator $\hat{P}_k$. Note that, as above, $|\Phi_{\mathrm{UHF}}\rangle$ is simply a computational basis state (although we implicitly work in two different bases). We can therefore make a controlled preparation of $|\Phi_{\mathrm{UHF}}\rangle$ from the vacuum state using a single CNOT gate for each occupied orbital, as shown in Fig. 2. Let $C\text{-}U_{\mathrm{UHF}}$ denote the set of CNOT gates that prepares $|\Phi_{\mathrm{UHF}}\rangle$ conditional on the state of an ancilla qubit and let $C\text{-}P_k$ denote the controlled-P_k gate. Due to the fact that $e^{\hat{\tau}_I}$, $\hat{\mathcal{U}}_{I\to 1}$, $\hat{\mathcal{U}}_{J\to 1}^\dagger$, and $e^{-\hat{\tau}_J}$ all conserve particle number, we have the following equality:

$$\begin{aligned}&(C\text{-}U_{\mathrm{UHF}})^\dagger e^{-\hat{\tau}_J} \hat{\mathcal{U}}_{J\to 1}^\dagger (C\text{-}P_k) \hat{\mathcal{U}}_{I\to 1} e^{\hat{\tau}_I} (C\text{-}U_{\mathrm{UHF}}) |+\rangle |\mathrm{vac}\rangle \\ &= \frac{1}{\sqrt{2}} \big(|0\rangle |\mathrm{vac}\rangle + U_{\mathrm{UHF}}^\dagger e^{-\hat{\tau}_J} \hat{\mathcal{U}}_{J\to 1}^\dagger \hat{P}_k \hat{\mathcal{U}}_{I\to 1} e^{\hat{\tau}_I} |1\rangle |\Phi_{\mathrm{UHF}}\rangle\big).\end{aligned} \tag{24}$$

A quick computation verifies that measuring the ancilla qubit in the X basis yields the quantity

$$\mathrm{Re}\big(\langle \Phi_{\mathrm{UHF}}| e^{-\hat{\tau}_J} \hat{\mathcal{U}}_{J\to 1}^\dagger \hat{P}_k \hat{\mathcal{U}}_{I\to 1} e^{\hat{\tau}_I} |1\rangle |\Phi_{\mathrm{UHF}}\rangle\big), \tag{25}$$

as desired. The imaginary part can be estimated in the usual way, by beginning with the ancilla state in the -1 eigenstate of the Pauli Y operator (see Sec. S3 of the Supplemental Material [68]).

On real quantum hardware, the matrix elements of the Hamiltonian and overlap matrix would be evaluated by repeatedly running the NOQE circuit of Fig. 1 or Fig. 2, as in Ref. [26]. However, for this first accuracy-benchmarking study of the NOQE approach on small molecules, we evaluate the matrix elements by use of a quantum simulator to generate representations of the ansatz states $|\phi_J\rangle = \hat{\mathcal{U}}_{J\to 1} e^{\hat{\tau}_J} |\Phi_J\rangle$ in the 2^N-dimensional vector space of FCI determinants. We then simulate the idealized (i.e., noiseless) circuit result classically, by directly evaluating the bitwise inner product $\langle \phi_I | \hat{H} | \phi_J \rangle$.

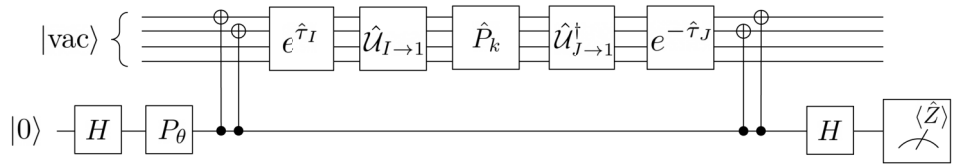

FIG. 2. The NOQE circuit for evaluation of the off-diagonal matrix elements with fewer qubits. Here, $\hat{P}_k$ arises from a decomposition of the Hamiltonian (expressed in the Ith UHF basis) in terms of Pauli operators. For the phase gate P_θ, we set $\theta = 0$ ($P_\theta = I$) when measuring $\mathrm{Re}(H_{IJ})$ and $\theta = \pi/2$ when measuring $\mathrm{Im}(H_{IJ})$ (see Sec. S3 of the Supplemental Material [68]).

D. Technical details

We use OpenFermion [91], PySCF [92], and QChem [93] to generate the reference states used in the NOQE protocol. Both OpenFermion and OpenFermion-PySCF are augmented to allow unrestricted Hartree-Fock (UHF) states to be prepared. The UHF solutions themselves are obtained via the Q-Chem 5 software package [93]. These solutions to the Hartree-Fock equations are obtained with the following procedure:

(1) Optimize the restricted open-shell Hartree-Fock solution with all radical sites having unpaired electrons and all unpaired spins pointing in the same direction. For H_2, this is the triplet state; for H_4, it is the quintet state.
(2) Spatially localize this first set of orbitals [94,95]. Hartree-Fock equations can at times yield spurious results with spins in delocalized orbitals, especially for species such as H_4 [96], so this step removes that possibility. Ensure that the orbitals are localized such that physically identifiable determinants are obtained as basis states. We note that for H_2 there is no scope for standard localization procedures [94,95], since only one orbital of each spin is occupied. For H_4 in the STO-3G basis, we obtain local solutions by using an initial guess that consists of one spin-up electron in each of the four $1s$ orbitals and then optimized with square-gradient minimization (SGM) [97], an algorithm that largely preserves the local nature of the orbitals.
(3) Generate all possible permutations of up and down spins (on these radical sites) that have the desired total m_s value (equal to zero in this work, unless specified otherwise). For H_2 with $m_s = 0$, there are only two radical sites possible for one up and one down spin, leading to two determinants. For $m_s = 0$ H_4, there are four radical sites, on which two up and two down spins have to be placed, resulting in six possible spin configurations and hence six determinants. These spin arrangements for H_2 and H_4 are shown in Fig. 3.
(4) Optimize unrestricted Hartree-Fock states corresponding to these permuted electronic configurations, by using the determinants from the previous step (that utilize restricted open-shell orbitals) as the initial guess. The SGM algorithm is used for this optimization to ensure that the closest stationary state to the initial starting point is reached. The resulting unrestricted Hartree-Fock solutions are used for NOQE applications. We note that other physically reasonable localization procedures or choices of initial orbitals other than ROHF could be used, although there will be no difference because each optimized UHF determinant is a well-defined stationary point in the orbital Hilbert space. The key is to be already in the quadratic basin of each stationary point with the initial guess.

The above procedure is similar to the manner in which reference determinants for the classical spin-flip (SF) NOCI method are generated [50]. To briefly summarize the SF-NOCI procedure, an active space is selected and then an automated code performs spin flips within this active space starting from a high-spin reference, in order to generate all possible configurations with, e.g., $m_s = 0$. Next, the active orbitals are frozen and the rest of the occupied orbitals in each configuration are allowed to relax. This yields a set of nonorthogonal Slater determinants where the core electrons have been allowed to polarize in order to accommodate, e.g., an ionic configuration that might have significant weight in the multireference wave function. In contrast to this SF-NOCI procedure, in NOQE no orbitals have to be held frozen and full orbital relaxation can be carried out on account of advancements in classical algorithms for optimizing orbitals [98].

In this work, we consider systems with d radical sites and $\eta = d$ electrons within the total $m_s = 0$ subspace. As is shown, using only the $m_s = 0$ subspace to describe eigenvectors with different $\langle\hat{S}^2\rangle$ (i.e., singlet, triplet, quintuplet, ...) leads to advantageous cancelation of errors in the energy gaps between these states. Therefore, we have exactly $d/2$ up and $d/2$ down spin electrons. The total number of NOQE reference states M is then equal to

$$M = \frac{d!}{\left(\frac{\eta}{2}!\right)^2} \tag{26}$$

determinants. For the general case with d radical sites, η_α up spins and η_β down spins (where $\eta_\alpha + \eta_\beta < d$, $m_s = \eta_\alpha - \eta_\beta$), the number of NOQE reference states is given by

$$M = \frac{d!}{\eta_\alpha!\eta_\beta!(d-\eta_\alpha-\eta_\beta)!}. \tag{27}$$

The low-rank circuits that prepare the NOUCC(2) reference states for NOQE are compiled using CIRQ [99]. The full circuit for calculating the off-diagonal elements between NOQE reference states is shown in Sec. III C. However, as noted there, for the benchmark calculations presented in this work, we evaluate the matrix elements directly in the computational basis and do not take into effect the quantum measurement noise or circuit noise, which would be present in experimental evaluation of the off-diagonal matrix elements. This is consistent with our goal in this work of establishing the ideal values possible under a NOQE calculation.

IV. RESULTS

A. Hydrogen molecule

At its minimum-energy geometry, the H_2 molecule has an internuclear separation ("bond length") of 0.74 Å. The wave function at this geometry is well approximated by a single RHF Slater determinant in which both electrons occupy the same bonding spatial orbital. This RHF determinant is, however, incapable of describing the dissociation limit of two independent H atoms (see Sec. S1D of the Supplemental Material [68]). Indeed, the optimal single determinant description for the dissociation limit of H_2 consists of two independent atoms with one electron localized around each. There are thus two UHF states possible, corresponding to the two possible ways to arrange an up and a down spin on the two atoms without spin pairing (as shown in Fig. 3).

The behavior at internuclear distances between these two limits is intermediate between them. The RHF determinant continues to be the minimal-energy Hartree-Fock solution for internuclear separations smaller than a cutoff distance that is commonly referred to as the Coulson-Fischer (CF) point [100]. Beyond the CF point, however, it is energetically favorable to (partially) unpair the two electrons. The minimum-energy Hartree Fock solutions are then spin-symmetry-broken UHF determinants wherein the individual atoms have nonzero net spin. There are two such energetically degenerate UHF states because the net spin on a particular atom can point either up or down (with the net spin on the other atom being in the opposite direction to preserve total $m_s = 0$). The spin-symmetry breaking in these UHF states prevents them from being eigenstates of the $\hat{S}^2$ operator and instead causes them to be a mixture of singlet and triplet states. The minimum-energy Hartree Fock solution thus branches from a single RHF determinant to two (overlapping) UHF determinants at the CF point. This branching is continuous in both the energy and its first derivatives, with discontinuities arising only in the second derivatives of the energy, at the CF point [101]. The two spin-symmetry-broken UHF states, therefore, have an overlap that is close to 1 just beyond the CF point (having barely branched from the same parent RHF state) but is equal to 0 at an infinite internuclear distance.

These branching UHF states constitute our NOUCC(2) reference states at distances beyond the CF point. They recouple to yield the lowest-energy singlet (S_0) and lowest-energy triplet (T_1) states in an approximately spin-pure manner. Potential singularities in the **S** matrix are removed by discarding singular values less than 10^{-4}. At distances shorter than the CF point, the RHF state is the only possible reference state. This has the consequence that the T_1 state appears only beyond the CF point where there are two reference states, while the S_0 state can be described by the RHF state and is thus also found at shorter distances. We note that the inability of this chosen set of reference states to model the T_1 state at small internuclear distances is not particularly limiting, because the T_1 state is very high in energy relative to the S_0 ground state in this regime and the ordering of the spin states is not in doubt here. Indeed, the electronic structure in this "single-reference" regime is well described by classical methods [102]. The description of the ground and excited states beyond the CF point is more challenging due to spin-symmetry breaking [36,101,103]. We note that the precise location of the CF point has a slight dependence on the basis set utilized but has a finite limiting value as the basis-set size is increased to the complete basis-set limit. Further discussion about the CF point is provided in Sec. S1D of the Supplemental Material [68].

Since there are (at most) two reference states in this description of H_2, only a single off-diagonal matrix-element energy evaluation is needed. Given a single-particle basis size of N spin orbitals, we note that $2N + 1$ qubits are needed to construct the NOQE circuit in Fig. 1 or $N + 1$ qubits for the circuit shown in Fig. 2. We carry out calculations with three basis sets, namely, STO-3G [104], 6-31G [105], and 6-311G [106]. The following discussion is based on results obtained with the 6-311G basis. Results obtained with the other two basis sets show comparable results and are presented in Sec. S5 of the Supplemental Material [68]. The number of basis functions per hydrogen atom, the number of spin orbitals (N), and the total number of qubits required to construct the NOQE circuit of Fig. 1 are listed in Table I. The resulting circuit depths (number of layers of parallel gate operations) for these calculations employing the low-rank factorization of the doubles tensor operator $\hat{\tau}$ are listed in Table II.

Figure 4 presents the computed NOQE absolute energies for the S_0 [Fig. 4(a)] and the T_1 [Fig. 4(b)] eigenstates

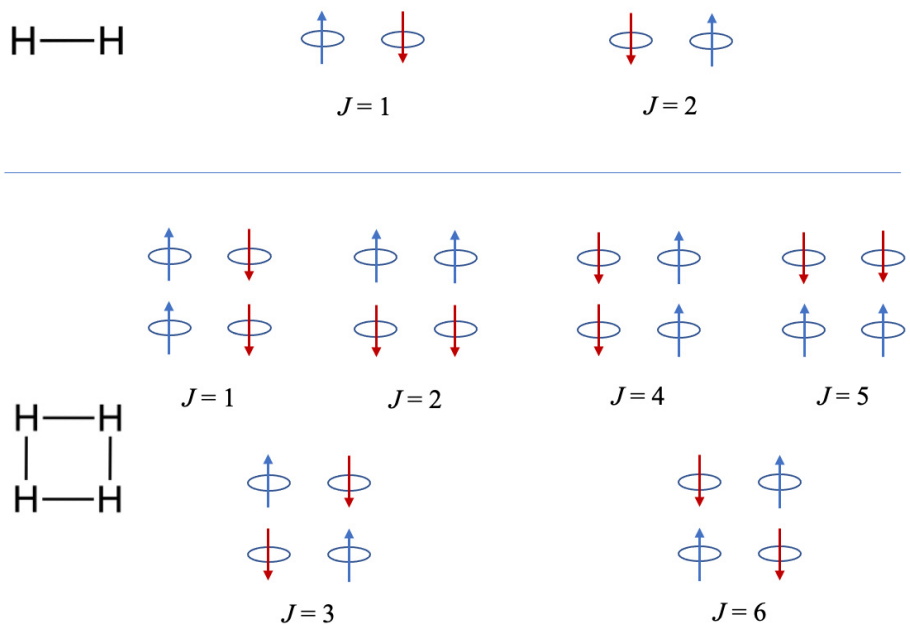

FIG. 3. UHF reference configurations for H_2 and square H_4 at the dissociation limit, showing the spatial distribution of spins on individual H atoms.

as a function of the internuclear separation, for calculations using the NOUCC(2) ansatz with the 6-311G basis set. Classical NOCI results without dynamic correlation, i.e., without MP2 amplitudes, and the exact FCI results are also provided for comparison. We observe that NOQE with NOUCC(2) provides a significant improvement on classical NOCI at all distances for both the S_0 and T_1 eigenstates, yielding a much closer approximation to FCI. In particular, the NOQE S_0 result smoothly traverses the CF point and is successful in removing the spurious second local minimum just beyond the CF point that is evident in the classical NOCI S_0 state. Indeed, the results from NOQE with the NOUCC(2) ansatz are qualitatively in good agreement with FCI at all internuclear distances.

We now consider quantitative accuracy, showing first the energy error relative to the FCI results in Fig. 5(a). We see that the NOQE S_0 and T_1 state energies differ from FCI by more than chemical accuracy at most distances and that the error is below chemical accuracy only at larger internuclear separations, where the system becomes increasingly well approximated by two independent atoms. The maximum error for the S_0 state is about 8 mHa, right around the CF point.

In practice, however, quantum chemists are seldom interested in absolute energies and instead prefer to look at energy differences between states (commonly referred to as "relative energies"). The most chemically relevant quantity for H_2 is therefore the energy difference between the S_0 and T_1 states (i.e., the "singlet-triplet gap," which we define here as $E_{T_1} - E_{S_0}$). Since NOQE with the NOUCC(2) ansatz overestimates the absolute energies of both the S_0 and T_1 states (see Fig. 4), this can lead to some cancelation of systematic error for the singlet-triplet gap. This is shown in Fig. 5(b), which shows that for the 6-311G–basis calculation, the magnitude of the singlet-triplet gap error is lower than the absolute energy errors at all internuclear distances. Around the CF point, it is less than 4 mHa, about half of the absolute error in S_0. Furthermore, the maximum singlet-triplet gap error decreases as the basis-set size of the calculation is increased from STO-3G to 6-31G to 6-311G, suggesting that larger more physically accurate basis sets such as cc-pVDZ (with five basis functions per H atom, resulting in 20 spin orbitals) could yield even lower errors. This is discussed in more detail in Sec. S5C of the Supplemental Material [68].

We now consider the impact of scaling the MP2 parameters on these results, which has been found to be beneficial

TABLE II. The circuit depth of the (full-rank) ansatz-preparation unitary operator $\hat{\mathcal{U}}_{J\to 1}e^{\hat{\tau}_J}$ with MP2 amplitudes, i.e., NOUCC(2), for H_2 with increasing basis-set size. These ansatz preparations may be performed in parallel, as in Fig. 1, or in sequence, as in Fig. 2.

Basis set	Circuit depth (SVD)	Circuit depth (Takagi)
STO-3G	53	38
6-31G	386	255
6-311G	1061	864

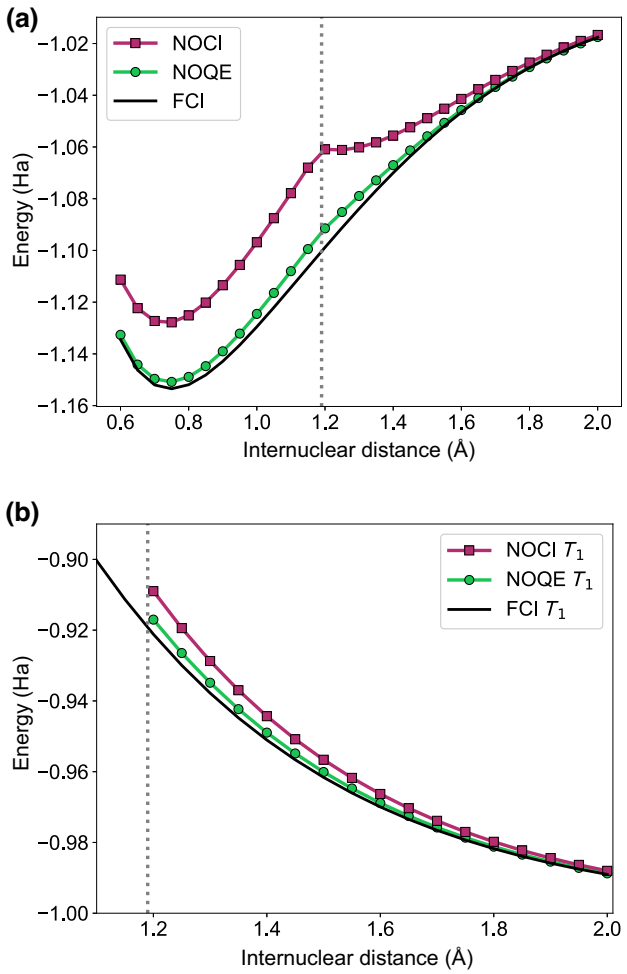

FIG. 4. A comparison of the NOUCC(2) and FCI eigenenergies for H_2, with the 6-311G basis set. Classical NOCI results (without dynamic correlation) are also provided for comparison. The location of the Coulson-Fischer (CF) point (1.19 Å for the HF state in the 6-311G basis) is marked as a dotted gray line. Note that the T_1 state only appears beyond the CF point for NOCI and NOUCC(2) calculations. (a) The lowest-energy singlet (S_0) state. (b) The lowest-energy triplet (T_1) state.

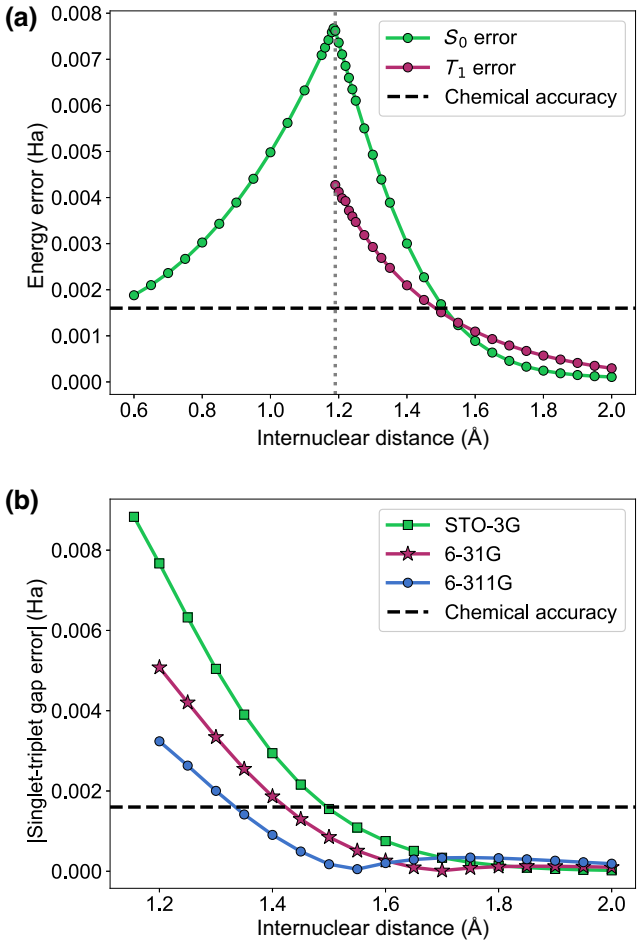

FIG. 5. Errors in energies relative to FCI for H_2 from NOQE with the NOUCC(2) ansatz states. The location of the CF point is marked with a dotted gray line in Fig. 5(a) but not in Fig. 5(b), since the precise location of this point depends slightly on the basis used. (a) The error in the S_0 and T_1 eigenenergies with the 6-311G basis. (b) The magnitude of the error in the singlet-triplet gap with different basis sets.

in classical quantum chemistry [61,62]. Therefore, we investigate the effect of uniformly scaling MP2 amplitudes by scaling parameters $s = 1.2$ and 1.3, as suggested classically by SCS- and SOS-MP2 (Sec. III B 1). We note that for H_2 with UHF states derived from the reference configurations of Fig. 3, there are no same-spin amplitudes, so only the opposite-spin amplitudes are relevant. Figure 6 shows that the use of scaled MP2 amplitudes can significantly lower the errors in both absolute energies and the singlet-triplet gap. Indeed, the scaled MP2 amplitudes for scalings $s = 1.2$ and $s = 1.3$ now yield singlet-triplet gaps within chemical accuracy from FCI at all internuclear distances [Fig. 6(b)]. Improvement of the S_0 absolute energies is less dramatic but still quite significant, with calculations for $s = 1.3$ almost halving the maximum error.

We are also interested in ascertaining the quality of approximation of the NOQE states to the true FCI states. To this end, we define the state infidelity

$$I_{\mathrm{FCI}} = 1 - |\langle \Psi_{\mathrm{NOQE}} | \Psi_{\mathrm{FCI}} \rangle|^2, \tag{28}$$

which is the fraction of the FCI state not captured by NOQE. Figure 7 shows the infidelities I_{FCI} of the singlet and triplet NOQE states as a function of the internuclear distance. The maximum infidelity over all distances is approximately 1% (at the CF point) without any amplitude scaling and is further reduced on scaling the amplitudes with $s > 1$. This indicates that both the S_0 and T_1 states are reproduced to approximately 99% or better fidelity by NOQE with the NOUCC(2) ansatz. We also note that the NOQE states also show a high degree of spin purity, with

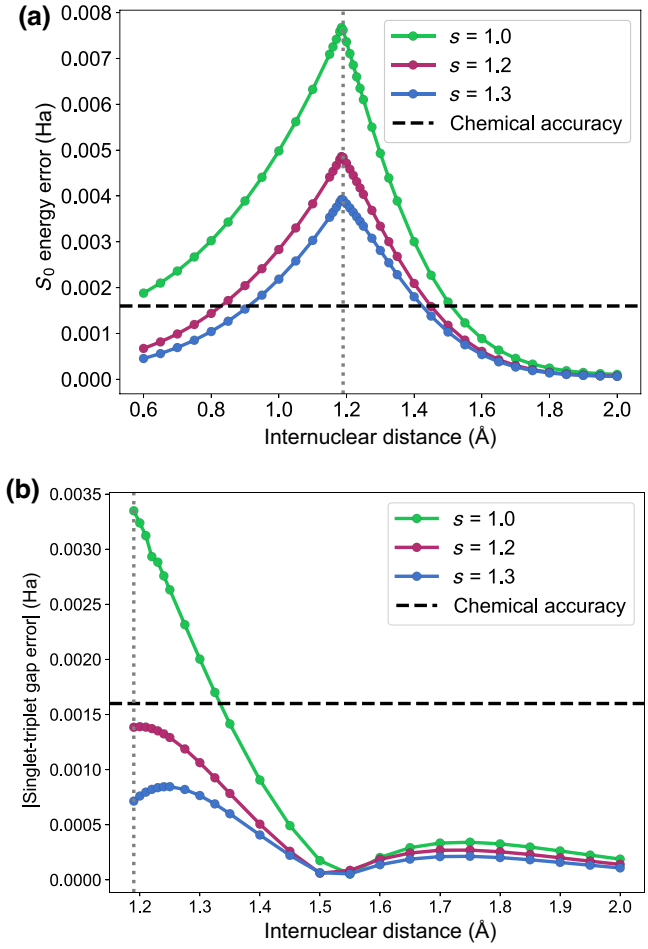

FIG. 6. Energy errors relative to FCI for singlet and triplet states of H_2 from NOQE with NOUCC(2) ansatz states in which the MP2 amplitudes are scaled by s (calculations made with the 6-311G basis). The location of the CF point is marked with a dotted gray line. (a) The S_0 energy error relative to FCI. (b) The magnitude of the error in the singlet-triplet gap, relative to FCI.

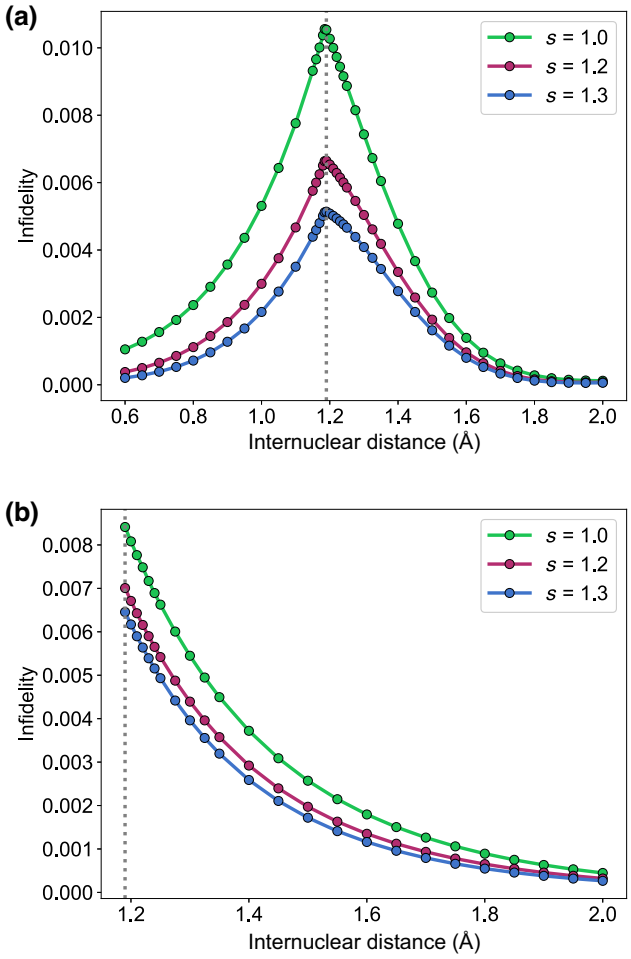

FIG. 7. The infidelity I_{FCI} relative to the FCI states of the amplitude scaled NOQE states derived from the NOUCC(2) ansatz, for H_2 with the 6-311G basis [see Eq. (28)]. The location of the CF point is marked with a dotted gray line. (a) The infidelity of the NOQE S_0 state. (b) The infidelity of the NOQE T_1 state.

a maximum error of 3×10^{-7} in $\langle \hat{S}^2 \rangle$ against FCI over the same range of internuclear distances.

B. Square H_4 system

We now consider a system that is considerably more challenging for classical methods, namely, the square geometry H_4 species, in which all four H atoms are equivalent. While the formation of H_4 from separate H_2 molecules is energetically unfavorable, the square H_4 molecule represents a benchmark system for quantum chemical studies of strong electron correlation. In particular, for short side lengths, square H_4 is a model for more complex antiaromatic molecules such as cyclobutadiene, which possesses a triplet ground state. However, longer side lengths lead to singlet ground states with four strongly correlated electrons. The switch from a triplet ground state to a singlet ground state occurs at 0.82 Å in the STO-3G basis, although the two states remain fairly close in energy in the neighborhood of the crossover point (with the singlet-triplet gap changing from −5 mHa at 0.76 Å side length to 5 mHa at 0.88 Å).

At the dissociation limit for total spin $m_s = 0$, there are four independent H atoms, two of which have up spins and two down spins, leading to six possible arrangements, each of which corresponds to a separate UHF state. These six UHF states are depicted in Fig. 3 and correspond to all possible spin arrangements without pairing. At shorter side lengths, an analogous set of UHF solutions is targeted and constructed using the protocol of Sec. III D. Unlike the situation for H_2, where the two possible UHF states are always degenerate for all internuclear distances, for H_4 the six possible UHF states for H_4, which are shown in Fig. 3, are not degenerate for all values of the side length.

The $J = 3$ and $J = 6$ states form a doubly degenerate set corresponding to the UHF global minimum, while the $J = 1, 2, 4, 5$ states form another degenerate set of higher energy. Detailed analysis shows that in the STO-3G basis, for side length less than 1.105 Å, the $J = 1, 2, 4, 5$ UHF states collapse to two closed-shell RHF states, reflecting a spin-pairing symmetry analogous to that found at the CF point for H_2, while for larger distances all six UHF states are linearly independent. The side length of 1.105 Å is not strictly speaking a CF point, because not all determinants show the transition in this case. However, it is a close analog to this and we refer to it as the CF point for H_4 in the STO-3G basis.

In contrast to the situation for H_2, the minimum-energy point for H_4 now lies well within the six-determinant spin-symmetry-broken regime, rather than in the spin-paired regime (see Fig. 8).There are at most six UHF states to consider and thus no more than 15 off-diagonal sets of matrix elements need to be made for all values of the side length. Since the NOQE calculations remove linear dependencies around the CF point by discarding the overlap-matrix singular values of 10^{-4} or less, in practice this number can be smaller for some distances. The number of basis functions per hydrogen atom, the number of spin orbitals (N), and the total number of qubits required to construct the NOQE circuit of Fig. 1 for H_4 with the STO-3G basis are listed in Table I. The corresponding circuit depths employing the low-rank factorization the two-body excitation tensor operator $\hat{\tau}$ are listed in Table III.

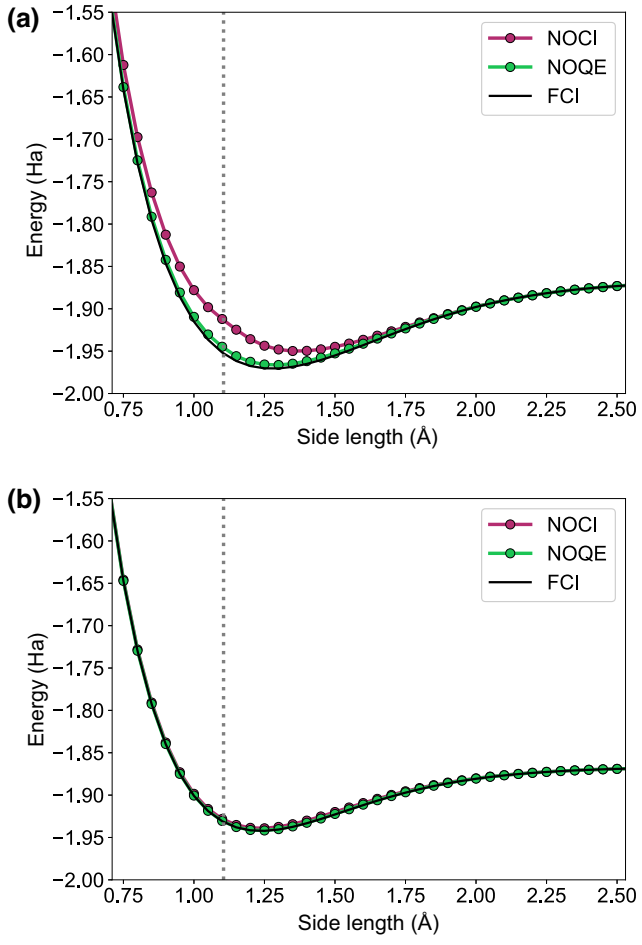

FIG. 8. A comparison of the NOUCC(2) and FCI eigenenergies for H_4, with the STO-3G basis set. Classical NOCI results (without dynamic correlation) are also provided for comparison. The location of the CF point (1.105 Å for the HF state in the STO-3G basis) is marked as a dotted gray line. Note that the T_1 state only appears beyond the CF point for the NOCI and NOUCC(2) calculations. (a) The lowest-energy singlet (S_0) state. (b) The lowest-energy triplet (T_1) state.

TABLE III. The circuit depth of the (full-rank) ansatz-preparation unitary operator $\hat{\mathcal{U}}_{J\to 1}e^{\hat{\tau}_J}$ with MP2 amplitudes, i.e., UCC-MP2, for the six reference states of H_4 shown in Fig. 3, in the STO-3G basis. The $J = 3$ and $J = 6$ states require lower circuit depths, as the MP2 amplitudes corresponding to correlation between spins of the same sign are zero from symmetry. These ansatz preparations may be performed in parallel, as in Fig. 1, or in sequence, as in Fig. 2.

Reference state J	Circuit depth (SVD)	Circuit depth, (Takagi)
1	555	371
2	594	386
3	283	183
4	593	399
5	583	390
6	281	183

Figure 8 shows the NOQE potential-energy surface for the S_0 and T_1 states of square H_4 using the NOUCC(2) ansatz with the STO-3G basis and Fig. 9(a) shows the corresponding energy errors for both states. We see that NOQE and FCI agree very well for these states, while classical NOCI proves to be quite inadequate at shorter side lengths for the S_0 state. Figure 9(a) reveals that the energy difference between NOQE and FCI for the S_0 state is similar to that observed for H_2, with a maximum deviation around 7 mHa near the CF-point analog for H_4. However, we note that the T_1 state has a very low deviation from FCI, being within chemical accuracy at all side lengths.

The lowest-energy quintet (Q_1) state shows very interesting behavior. Figure 9(a) shows that the error against FCI is quite low at longer bond lengths but in contrast to the behavior of the S_0 and T_1 errors, the quintet Q_1-state energy error rises dramatically as the CF point is approached. This behavior has a physical interpretation, namely, the consequence of increasing spin contamination as the side length shortens. At side lengths shorter than the CF point H_4 in the STO-3G basis at 1.105 Å side length, the NOUCC(2) subspace of reference states

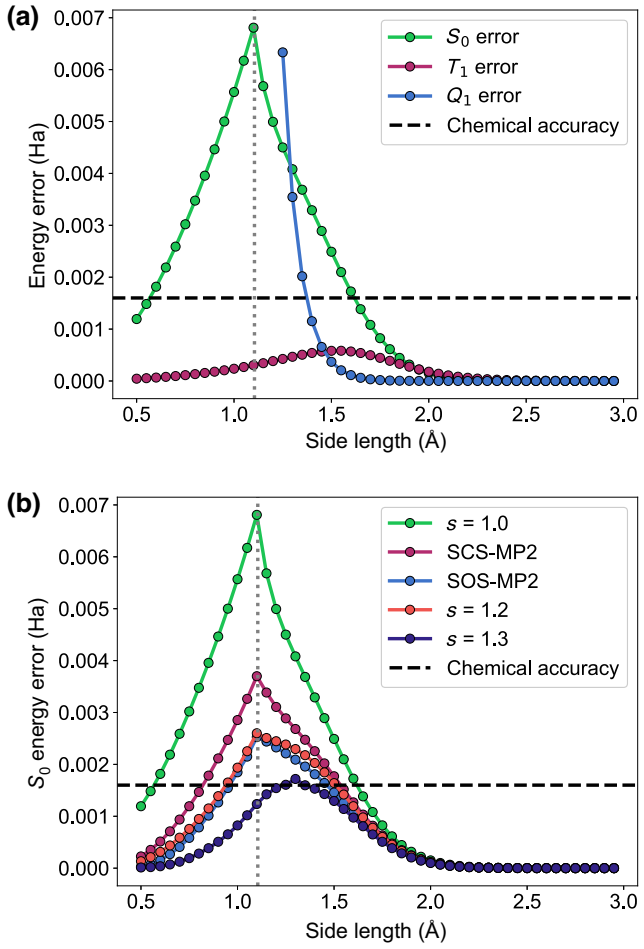

FIG. 9. Errors in energies relative to FCI for square H_4 from NOQE with the NOUCC(2) ansatz states. The location of the CF point is marked with a dotted gray line. (a) Errors in the S_0, T_1, and Q_1 NOQE energies with the NOUCC(2) ansatz. (b) The NOQE S_0 energy errors for the NOUCC(2) ansatz with scaled MP2 $\{t_{abij}\}$.

provides an inadequate description of the Q_1 state, because the former is targeting the low-energy states, while the Q_1 state is very high in energy relative to the T_1 and S_0 states. Indeed, the state with the greatest quintet character deriving from the NOQE calculation with the NOUCC(2) ansatz in this regime is a heavily spin-contaminated state with $\langle \hat{S}^2 \rangle \sim 4 - 5$, which is a poor approximation to the true Q_1 state, for which $\langle \hat{S}^2 \rangle = 6$. This heavily spin-contaminated state is best viewed not as a proper eigenstate but, rather, as the residue left in the NOQE subspace after the lower energy S_0 and T_1 states have been solved for, with the high degree of spin contamination being a mark of its poor quality. However, when the side length is stretched, the Q_1 energy is lowered and the state is then better captured by the NOUCC(2) ansatz. Thus, for a side length greater than 1.25 Å, the absolute spin contamination in the highest-energy NOQE state is reduced to 0.05 or less, i.e., $\langle \hat{S}^2 \rangle \geq 5.95$. The state can be reasonably labeled as Q_1 from that point on but not at shorter distances due to greater spin contamination and therefore we do not plot Q_1 at the shorter bond lengths in Fig. 9(a) or elsewhere. This example indicates that the extent of spin contamination provides a useful internal check on the accuracy of the NOQE energies.

The energy errors in the S_0 state can be further reduced by scaling the MP2 amplitudes, as shown in Fig. 9(b). Since both same-spin and opposite-spin MP2 amplitudes are present for H_4 with $m_s = 0$, we investigate the behavior of both the SCS- and SOS-MP2 models, as well as their uniform-scaled analog. Figure 9(b) shows that uniform scaling of the MP2 amplitudes yields the lowest error, with a value of $s = 1.3$ bringing the NOQE ground-state singlet S_0 energy error below chemical accuracy for all internuclear distances. We do not separately examine the behavior of the singlet-triplet gap, as the much lower error in the T_1 energy for this basis set [as shown in Fig. 9(a)] indicates that it would look very similar to the S_0 energy error plot.

We also evaluate the extent of spin contamination in the S_0 state, shown in Fig. 10(a). $\langle \hat{S}^2 \rangle$ is below 0.01 even with the unscaled approach, indicating quite low error versus the exact value of $\langle \hat{S}^2 \rangle = 0$. Scaling reduces the error further. The error in $\langle \hat{S}^2 \rangle$ for the T_1 state (not shown) is considerably lower (maximum deviation of 5×10^{-6}), showing that the low-energy S_0 and T_1 states are modeled in a nearly spin-pure fashion by NOQE with the NOUCC(2) ansatz. On the other hand, the higher-energy Q_1 state shows greater levels of spin contamination, having $\langle \hat{S}^2 \rangle < 5.94$ (in the unscaled case) at distances shorter than 1.25 Å against the exact value of $\langle \hat{S}^2 \rangle = 6$. Indeed, $\langle \hat{S}^2 \rangle$ for the closest analog to the Q_1 state reaches 4–5 at side lengths shorter than the CF point, as previously noted. Interestingly, the SCS- and SOS-MP2 amplitudes worsen spin contamination for the Q_1 state at shorter side lengths (having error > 0.01 at 1.45 Å), as compared to unscaled or uniformly scaled results (which have approximately 0.006 error at by 1.45 Å).

We note that while spin purity is a necessary measure of the quality of the final NOQE states, it is not a sufficient one. Figure 10(b) shows the infidelity of the S_0 state for H_4, which reveals that NOQE with unscaled MP2 amplitudes in the NOUCC(2) reference states attains over 99% fidelity at all values of the side length of the molecule, with the scaled amplitude ansatz states showing even greater overlaps with the FCI eigenstate. Lower infidelity values are obtained for the T_1 state, being 0.08% or less in all cases. Even the Q_1 state shows infidelities approximately 1% or less for side lengths longer than 1.45 Å with the unscaled and uniformly scaled ansätze, although SCS- and SOS-MP2 amplitudes lead to greater infidelity (reaching approximately 2%) at 1.45 Å.

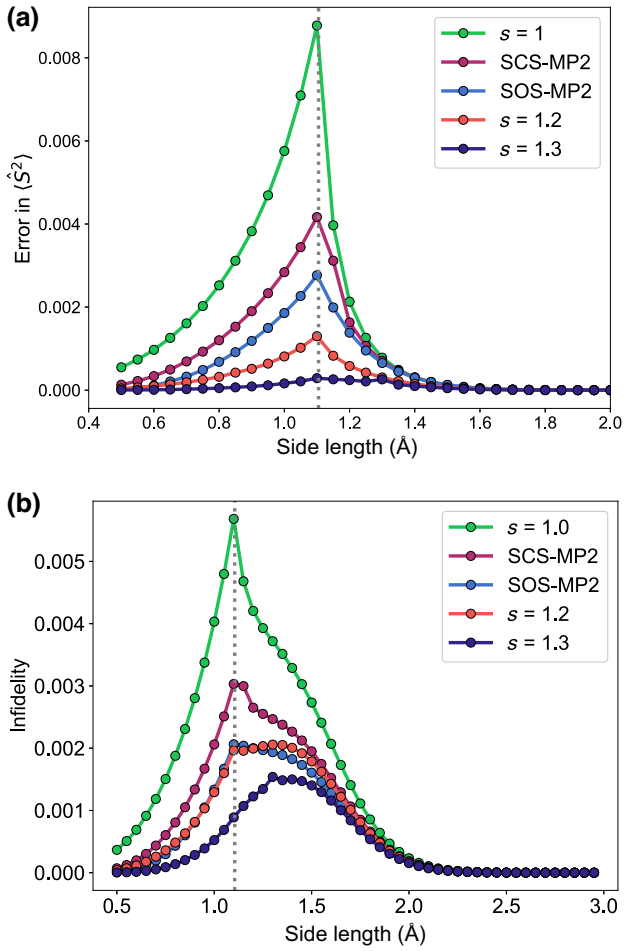

FIG. 10. The spin contamination error and state infidelity [I_{FCI}, Eq. (28)] relative to the FCI states of the amplitude-scaled NOQE states derived from the NOUCC(2) ansatz, for H_4 with the STO-3G basis. The location of the CF point is marked with a dotted gray line. (a) The error in $\langle \hat{S}^2 \rangle$ for the S_0 state. (b) The infidelity in the S_0 state.

C. NOUCJ for H_2 in the STO-3G basis

We also undertake a preliminary investigation of NOQE with the NOUCJ ($L = 1$) ansatz (for the remainder of this section, the $L = 1$ label is suppressed) by examining its performance for H_2 in the STO-3G basis. A comparison of the errors in the S_0 state (versus FCI) for the NOUCJ and NOUCC(2) ansätze is shown in Fig. 11. The T_1 state in this basis has zero correlation and is thus not considered. It appears that the maximum-energy error is lower for NOQE with the NOUCJ ansatz than the unscaled NOUCC(2) ansatz, although scaling NOUCC(2) amplitudes by 1.3 leads to even better performance. However, the error in the S_0 NOUCJ energy decays rather slowly with distance and remains above chemical accuracy until around 2 Å. In contrast, NOQE with NOUCC(2) shows a rapid decrease in error with increasing side length, going below the chemical accuracy threshold at around 1.5 Å.

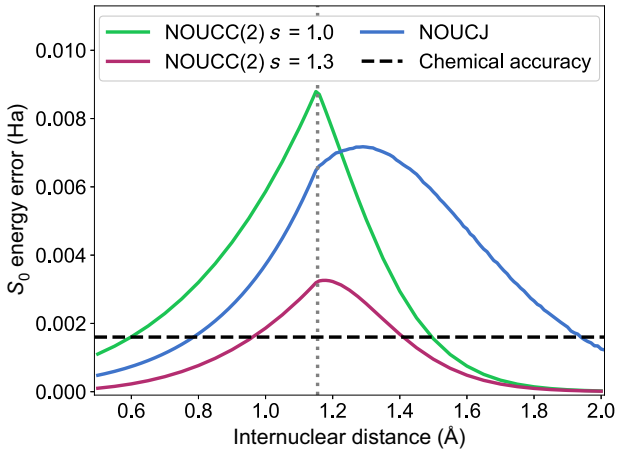

FIG. 11. A comparison of the S_0 energy errors with NOUCC(2) and NOUCJ ($L = 1$) against FCI for H_2 in the STO-3G basis. The location of the CF point (1.155 Å for H_2 in the STO-3G basis) is marked with a dotted gray line.

That said, increasing L beyond 1 (up to N^2) in the NOUCJ ansatz offers a route toward systematic improvement. As discussed further in Sec. V, the lower resource cost associated with the NOUCJ ansatz (particularly for the choice of $L = 1$) makes it very appealing for use in the NOQE framework, meriting further investigation.

D. Low-rank truncation for H_2 and H_4

The low-rank tensor decomposition of the cluster tensor Eqs. (3)–(5) that is given by Eq. (13) (for details, see Sec. S2 of the Supplemental Material [68]) allows for a systematic reduction of the NOQE circuit. For single-reference states, this can be done straightforwardly by truncation of the number of singular values L of the cluster tensor $\mathbf{T}$ to reduce its effective rank (the analogous truncation of ρ_L has been found to be less effective for the UCC operator [63]). We note that the error bounds presented in Sec. S4 of the Supplemental Material [68] may be used to guarantee a maximum NOQE energy error for a given choice of truncation. However, this is in practice a loose bound that overestimates the observed energy deviation when many singular values are discarded. While the L truncation strategy is not directly applicable to general multireference states, because each state may have a different truncation value, for H_2 the cluster operators for the two nonorthogonal reference states are equivalent by spin symmetry. In this situation, a single value of L can then be used for both reference states to analyze the effect of truncation on the NOQE energy.

Figure 12 shows, for H_2 with NOUCC(2), the dependence of the NOQE ground-state energy on the choice of truncation parameter L, using the Takagi decomposition of the cluster supermatrix $\mathbf{T}$, at the equilibrium internuclear distance [Fig. 12(a)] and at the CF point [Fig. 12(b)]. The

full-rank value is defined as $L_{\text{eff}} \leq N_{\text{occ}} N_{\text{virt}} = \eta(N-\eta)$ and is the residual number of singular values of $\mathbf{T}$ retained when all zero and near-zero singular values up to a certain fixed precision threshold (taken here as 10^{-12}) are discarded, i.e., the effective full rank of $\mathbf{T}$. Figure 12(a) demonstrates that, at the equilibrium bond length of 0.75 Å, we can truncate the circuit by setting $L = L_{\text{trunc}} = 11$ instead of $L = L_{\text{eff}} = 16$ and thus reduce the circuit depth, while remaining within chemical accuracy of the FCI result. Figure 12(b) shows the relatively more advantageous behavior of rank truncation when the bond is stretched to 1.2 Å (the CF point in the 6-311G basis). Although the full-rank NOQE energy lies slightly outside chemical accuracy, we find that the energy at truncated values of L converges more quickly to the full-rank result. This is because the longer bond distance enables the occupied and virtual orbitals to be more localized and reduces their mutual overlap, effectively lowering the rank of the $\mathbf{T}$ matrix.

For other multireference states, such as those of H_4, we must use an alternative truncation strategy to ensure consistency across the cluster tensor decompositions derived within UHF single-particle bases of different symmetry, which may have different L_{eff}. Since we are interested in the efficacy of the truncation procedure, we aim to find the minimum value of L, defined as L_{trunc}, for each single-reference state, such that truncating all cluster operators to their individual L_{trunc} values will yield an energy estimate within 1.6-mHa precision of the energy obtained using the full-rank cluster operators. Possible approaches include the use of a fixed tolerance threshold for the singular values of the cluster operator or, alternatively, a norm-based criterion as in Ref. [67]. Here, we employ a truncation strategy based on the vector ℓ^p-norms.

We compute the vector of ordered singular values $\vec{\sigma} = \text{diag}(\Sigma)$, where Σ is the diagonal matrix of singular values that results from SVD or Takagi decomposition of $\mathbf{T}$ (see Sec. S2 of the Supplemental Material [68]), and discard the largest subset of $L_{\text{eff}} - L$ singular values σ_l satisfying

$$\left(\sum_{l=L+1}^{L_{\text{eff}}} |\sigma_l|^p \right)^{1/p} \leq \varepsilon_p, \tag{29}$$

where ε_p is a variable threshold. Here, ε_p is the independent variable and L is the dependent variable to be determined. In this work, we use $p = 2$ and define $\varepsilon \equiv \varepsilon_2$. We first establish the values of L_{eff} for each of the reference states in the multireference ansatz and then perform a sweep over ε, truncating the vectors of singular values of each reference state according to Eq. (29), until we find the largest value of $\varepsilon = \varepsilon_{\max}$ that retains a desired level of accuracy in the multireference energy relative to the full-rank result. This sets the value of L_{trunc} for each of the reference states, from which the fractional reduction in circuit depth can then be estimated (see Sec. V).

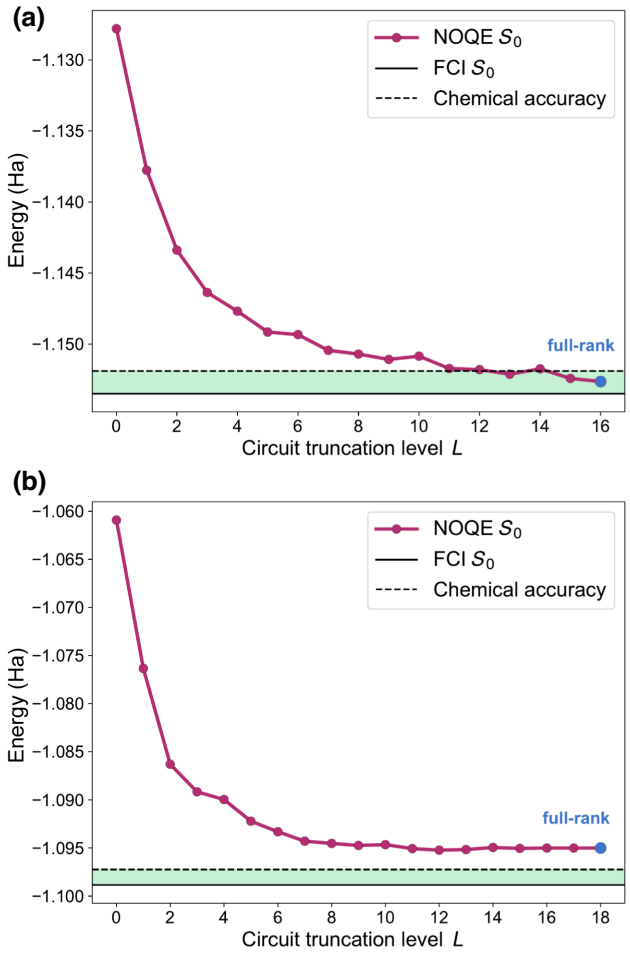

FIG. 12. The NOQE ground-state (S_0) energy dependence on the truncation level L of the cluster tensor, representing the circuit truncation level, for H_2 with $s = 1.3$ in the 6-311G basis set at the equilibrium bond distance [panel (a)] and at the CF point [panel (b)]. The blue point labeled "full-rank" shows the value L_{eff}. The green shaded region corresponds to the range of energy that is within chemical accuracy of the FCI result. (a) The NOQE energy versus L at 0.75 Å, the equilibrium bond distance of H_2. (b) The NOQE energy versus L at 1.2 Å (the CF point of H_2 in the 6-311G basis).

The left-hand panels of Fig. 13 show the NOQE ground-state energy dependence on the ℓ^2-norm threshold ε for H_2–6-311G at the equilibrium bond distance [Fig. 13(a)] and the CF point [Fig. 13(b)]. The right-hand panels of Fig. 13 show the corresponding plots for square H_4 in the STO-3G basis at the equilibrium geometry [side length 1.3 Å, Fig. 13(c)] and the CF point [side length 1.1 Å, Fig. 13(d)]. Because the rank truncation is not a variational procedure, it is possible that truncation can yield NOQE energies slightly below the true NOQE values in the full-rank regime. However, the energies are still

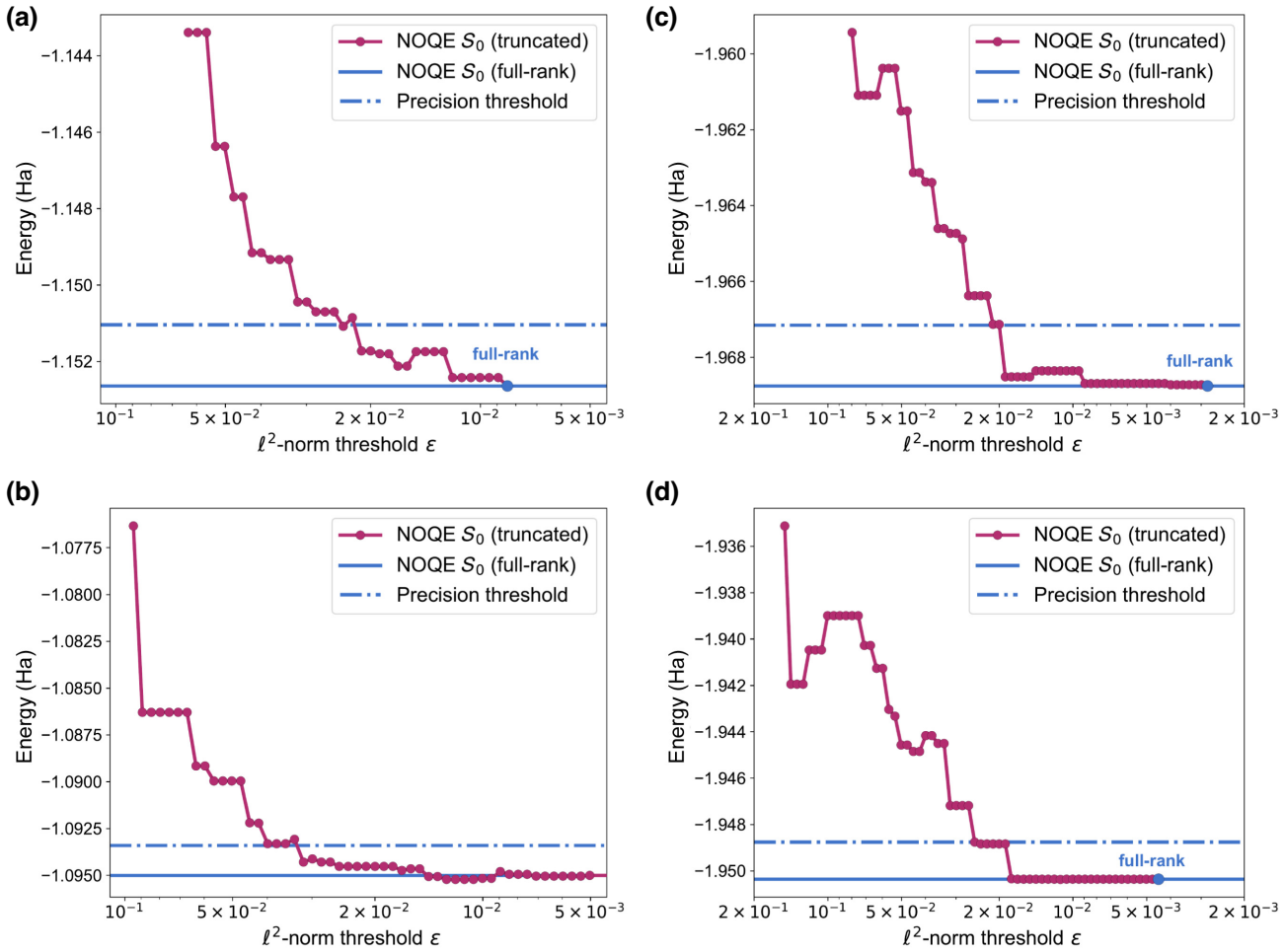

FIG. 13. The NOQE ground-state (S_0) energy dependence on the ℓ^2-norm threshold level ε, for H_2 in the 6-311G basis [panels (a) and (b)] and H_4 in the STO-3G basis [panels (c) and (d)], with $s = 1.3$ in their equilibrium geometries at their respective CF points. The blue points labeled "full-rank" and the solid blue lines show the values with untruncated circuits. The singular values σ_i of the cluster tensor that are removed by the ℓ^2-norm truncation are set to zero and the corresponding circuit blocks are then omitted, leading to savings in the circuit depth. (a) The NOQE energy versus ε at 0.75 Å (the equilibrium bond distance of H_2). (b) The NOQE energy versus ε at 1.2 Å (the CF point of H_2 in the 6-311G basis). The effects of truncation of the two smallest singular values ($\sigma_i \leq 10^{-4}$) give rise to energy changes of less than 1×10^{-6} Ha and are not shown in the plot. (c) The NOQE energy versus ε at 1.3 Å side length (the equilibrium bond length for square H_4). (d) The NOQE energy versus ε at 1.1 Å side length (the CF point for square H_4 in the STO-3G basis).

variational with respect to the FCI solution. For H_4 we can divide the reference states into two groups depending on the spatial distributions of the spins, as shown in Fig. 3. There are four configurations ($J = 1, 2, 4, 5$) in which the two spins of the same sign are on the same edge of the square and two ($J = 3, 6$) where the spins of the same sign are diagonally opposite each other on the square. For each group, we calculate the fractional circuit-depth reductions after truncation, $L_{\text{trunc}}/L_{\text{eff}}$, which we report in Table V. We also compute the total fractional reduction in the number of singular values over all references, $(\sum_{J=1}^{M} L_{\text{trunc}}^{(J)})/(\sum_{J=1}^{M} L_{\text{eff}}^{(J)})$, which we refer to here as the total cost reduction. We place emphasis on the single-reference circuit-depth reductions since they are directly related to the requisite coherence times of qubits on the quantum processor. However, it should be noted that the total cost reduction estimates are not directly related to the coherence time, because the circuits for different matrix elements can be run independently or in parallel on different sets of qubits. These estimates can instead be related to the total gate count (Sec. V). The total cost-reduction estimates are thus complementary to the single-reference circuit depths in discussing the overall effectiveness of rank truncation for a given NOQE system.

We observe a total cost reduction relative to the full-rank calculation of 18.8% and 15.6% at the equilibrium and the CF point, respectively (Tables IV and V). We note that different truncation methods (e.g., using a different ℓ^p-norm)

TABLE IV. Calculations of total circuit cost reduction for H_2 in the 6-311G basis (with $s = 1.3$) at the equilibrium distance (0.75 Å) and at the CF point (1.2 Å). For each calculation, the ℓ^2-norm threshold $\varepsilon_{\max}$ is selected so that any $\varepsilon \leq \varepsilon_{\max}$ will yield truncated energies lying within 1.6-mHa precision of the full-rank result. $J = 1, 2$ refer to the spin configurations for H_2 in Fig. 3.

Internuclear distance (Å)	ℓ^2-norm threshold	$L_{\text{trunc}}/L_{\text{eff}}$ $(J = 1, 2)$	Total cost reduction (%)
0.75	2.4×10^{-2}	9/16	43.8
1.2	2.8×10^{-2}	7/18	61.1

result in different estimates of $L_{\text{trunc}}/L_{\text{eff}}$ and thus different percentages of total circuit cost reduction.

Comparing the overall circuit-reduction estimates for H_2 in the 6-311G basis ($N = 12$ spin-orbitals) and H_4 in the STO-3G basis ($N = 8$ spin-orbitals), we see that the effectiveness of the low-rank truncation is larger for the greater basis-set size, in agreement with the conclusions of norm-based truncation in Ref. [63]. These results for H_2 and H_4 also suggest that the circuit reduction is more significant at larger distances, regardless of the relative location of the equilibrium and CF points. In general, the utility of low-rank decompositions is most apparent in cases where there are a large number of very small singular values. Thus, we could expect much greater reductions in circuit depth than those found here, when decomposing MP2 amplitudes corresponding to spatially localized occupied and virtual orbitals that are well-separated (or more generally, nearly orthogonal), as is the case in long saturated hydrocarbons.

V. CIRCUIT RESOURCE ESTIMATION

In this section, we evaluate quantum resource estimates for the low-rank factorized NOUCC(2) algorithm as a function of (i) the system size (taken as the number of spin orbitals N) and (ii) the number of radical sites d that are directly involved in the strong static electron correlation. Specifically, we are analyzing the circuit in Fig. 1, with the small modification that the basis rotation is relative, i.e., NO reference J is always rotated into I, $\hat{\mathcal{U}}_{J\to I}$, instead of a common global basis. The two approaches are equivalent but the relative rotation reduces the gate complexity by a constant factor for each off-diagonal matrix element evaluated.

TABLE V. Calculations of total circuit cost reduction for H_4 in the STO-3G basis (with $s = 1.3$) at the equilibrium side length (square with side length 1.3 Å) and at the CF point (square with side length 1.1 Å). The ℓ^2-norm threshold $\varepsilon_{\max}$ is selected for each calculation, so that any $\varepsilon \leq \varepsilon_{\max}$ will yield truncated energies lying within 1.6-mHa precision of the full-rank result. $J = 1, 2, 4, 5$ correspond to the "edge-parallel" spin configurations and $J = 3, 6$ to the "diagonal-parallel" spin configurations for H_4 in Fig. 3.

Side length (Å)	ℓ^2-norm threshold	$L_{\text{trunc}}/L_{\text{eff}}$ $(J = 1, 2, 4, 5)$	$L_{\text{trunc}}/L_{\text{eff}}$ $(J = 3, 6)$	Total cost reduction (%)
1.3	1.8×10^{-2}	10/12	6/8	18.8
1.1	2.4×10^{-2}	11/12	5/8	15.6

A. Circuit cost of multireference ansatz preparation

The number of NO reference states in this work is denoted as M. This scales binomially with the number of radical sites, or "active space orbitals," d, and the number of electrons η within the total $m_s = 0$ subspace, according to Eqs. (26) and (27). For example, for H_2 we have $M = \binom{2}{1} = 2$ reference states, while for H_4 we have $M = \binom{4}{2} = 6$. Recall that it is found to be advantageous (in terms of maximizing error cancelation in spin-gap quantities) when, for example, in the case of H_4, singlet, triplet, and quintet NOQE eigenstates are taken to be linear combinations of determinants in the $m_S = 0$ spin sector. The computation cost associated with classical diagonalization of an $M \times M$ matrix is therefore exponential with d (as also for classical NOCI) but for many difficult molecular applications of interest, we can expect the number of radical sites d to be less than ten. There will be M diagonal matrix elements of the NOQE Hamiltonian, $\mathbf{H}$, and $M(M-1)/2$ upper triangular matrix elements (not including the diagonals). One matrix element, H_{IJ}, requires two controlled $N \times N$ SWAP gates, two unitaries $e^{\hat{\tau}_I}$ and $e^{\hat{\tau}_J}$ to prepare the two NO reference states, and one additional unitary basis rotation $\hat{\mathcal{U}}_{J\to I}$ (we ignore the two Hadamard gates on the ancilla qubit).

When running quantum algorithms on NISQ devices, one critical quantity of interest is the number of two-qubit gates required, typically the CNOT gate count. We use the fact that a two-qubit Givens rotation, a paired number-operator rotation ($e^{-i\theta \hat{n}_p \hat{n}_q}$ with $p \neq q$), and a controlled-SWAP (CSWAP) gate require four, two, and eight CNOT gates, respectively. We note that the number-operator pair rotations would incur additional CNOT gates on a linear architecture in the form of a SWAP network to connect the non-neighboring qubit pairs [80,107]. However, in the current analysis, for simplicity, we assume full connectivity on the device.

Each $\hat{\mathcal{U}}_B$ basis rotation can be implemented with $2\binom{N/2}{2}$ Givens rotations, accounting for unrestricted orbitals. For the Ith UCCMP2 reference state, the number of basis-rotation operators is $1 + mL$ (where $L \leq \text{rank}(\mathbf{T})$ and the number of $\hat{Y}^2$ terms per singular value is $m = 4$ for SVD or $m = 2$ for Takagi, for a total of mL circuit blocks). Alternatively, with the UCJ approach in Eq. (15), only two basis rotations are needed (equivalent to $L = 1$). In each circuit block, there are $\binom{N}{2} = N(N-1)/2$ distinct number-operator pair products (excluding diagonal terms). The controlled $(N \times N)$-qubit SWAP will require N pairs

of CSWAP gates (eight CNOTs each). Therefore, the total number of CNOT gates can be decomposed into the following CSWAP, Givens, and number-operator terms:

$$N_{\mathrm{CNOT}}^{\mathrm{SWAP}} = 8 \times 2 \times 2N = 32N, \tag{30}$$

$$N_{\mathrm{CNOT}}^{\mathrm{Givens}} = 4 \times k \left(2 \times 2\binom{N/2}{2} \times (1+mL) + 2\binom{N/2}{2}\right), \tag{31}$$

$$N_{\mathrm{CNOT}}^{\hat{n}_p\hat{n}_q} = 2 \times k\binom{N}{2} \times mL \times 2 = 4kmL\binom{N}{2}. \tag{32}$$

Note that the $2\binom{N/2}{2}$ in Eq. (31) corresponds to the $\hat{\mathcal{U}}_{J\to I}$ term and that k is the kth-order Trotter-Suzuki decomposition.

The number of CNOT gates for one off-diagonal NOQE matrix element is then equal to

$$N_{\mathrm{CNOT}}^{H_{IJ}} = N_{\mathrm{CNOT}}^{\mathrm{SWAP}} + N_{\mathrm{CNOT}}^{\mathrm{Givens}} + N_{\mathrm{CNOT}}^{\hat{n}_p\hat{n}_q}, \tag{33}$$

while the number of CNOT gates required for a diagonal term, H_{II}, is

$$N_{\mathrm{CNOT}}^{H_{II}} = 4 \times 2\binom{N/2}{2} \times (1+mL) + N_{\mathrm{CNOT}}^{n_p n_q}/2. \tag{34}$$

Overall, the total number of CNOT gates, $N_{\mathrm{CNOT}}^{\mathrm{Total}}$, is then equal to

$$N_{\mathrm{CNOT}}^{\mathrm{Total}} = \frac{M(M-1)}{2} N_{\mathrm{CNOT}}^{H_{IJ}} + MN_{\mathrm{CNOT}}^{H_{II}} \in \mathcal{O}(M^2kN^2L). \tag{35}$$

A second important resource count is the number of single-qubit non-Clifford T-gates, which is relevant to both NISQ and fault-tolerant quantum devices, since these rotations enable universal quantum computation. Alternatively, a more general analogous quantity is the number of arbitrary single-qubit-rotation gates (e.g., R_z) which can be decomposed into a number of T gates scaling as $1.15\log_2(1/\epsilon_{\mathrm{syn}}) + 9.2$ with arbitrary synthesis error ϵ_{syn}, using the result from Ref. [108]. A single Givens rotation, a single number-operator product, and the controlled $(N \times N)$-qubit SWAP require $2N$, $3N$, and $7N$ R_z gates, respectively.

We now consider all $N(N+1)/2$ relevant number-operator products, including the diagonals, because the diagonal $\hat{n}_p\hat{n}_p$ terms contribute single-qubit rotations. In general, the number of R_z gates, N_R, for generating each Takagi-factorized UCCMP2 reference ansatz is

$$N_R^{\mathrm{SWAP}} = 7 \times 2 \times 2N = 28N, \tag{36}$$

$$N_R^{\mathrm{Givens}} = 2 \times k \left(2 \times 2\binom{N/2}{2} \times (1+mL) + 2\binom{N/2}{2}\right), \tag{37}$$

$$N_R^{\hat{n}_p\hat{n}_q} = 3 \times k\frac{N(N+1)}{2} \times mL \times 2 = 3kmLN(N+1). \tag{38}$$

The total number of R_z gates for evaluation of an off-diagonal matrix element of H is given by

$$N_R^{H_{IJ}} = N_R^{\mathrm{SWAP}} + N_R^{\mathrm{Givens}} + N_R^{\hat{n}_p\hat{n}_q} \tag{39}$$

and the number of R_z gates for evaluation of diagonal Hamiltonian matrix elements is

$$N_R^{H_{II}} = 2 \times 2\binom{N/2}{2} \times (1+mL) + N_R^{\hat{n}_p\hat{n}_q}/2. \tag{40}$$

Overall, including the dependence on the number of NO basis states, M, the total number of R_z gates can then be expressed as

$$N_R^{\mathrm{Total}} = \frac{M(M-1)}{2} N_R^{H_{IJ}} + MN_R^{H_{II}} \in \mathcal{O}(M^2kN^2L), \tag{41}$$

which scales the same as the CNOT gate complexity.

We can use these resource counts to provide an empirical estimate for the overall gate counts required to achieve chemical accuracy for a given molecular system. In the case of UCC, the asymptotic scalings of the two relevant truncation indices of Eq. (14) are $\mathcal{O}(N^2)$ for L and $\mathcal{O}(N)$ for ρ_L. Using the truncation thresholds that have been shown in Ref. [63] to preserve chemically accurate energies for alkane chains of increasing length (up to eight carbon atoms), we estimate that the implied scaling prefactors for L and ρ_L are 0.04 and 1, respectively. In other words, $L = 0.04N^2$ and $\rho_L = N$. In NOUCC(2), UCC amplitudes are replaced with amplitudes obtained from MP2, decomposed in an analogous way, and we assume that similar levels of compression will be achieved. The overall CNOT counts are plotted in Fig. 14 for two (H_2), four (square H_4), and six radical sites. Sizable reductions in gate count result due to the eigenvalue truncation procedure described above and we find that the addition of a single radical site increases the two-qubit gate count by approximately one order of magnitude. We note that the overall scaling of the R_z gate counts is very similar.

The use of the UCJ ansatz in our NOQE framework is likely to be relatively advantageous, especially from a resource-cost perspective. Recall that for H_2, NOUCJ($L = 1$) is sufficient to produce comparable accuracy to NOUCC(2) with an untruncated factorization of

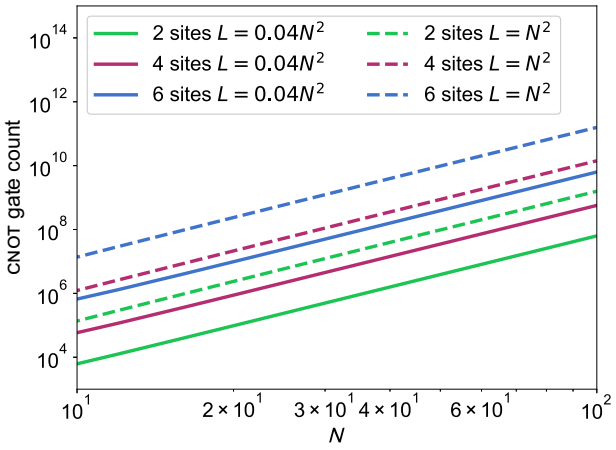

FIG. 14. The scaling of the number of two-qubit gates with the number of spin orbitals in the NOUCC(2) algorithm. Data for two, four, and six radical sites are shown. Without eigenvalue truncation, the L index is equal to N^2 (dotted lines). With a truncation threshold that preserves chemical accuracy for alkane chains up to eight C atoms, L can be as low as $0.04N^2$ (solid lines) [63].

the MP2 amplitudes. For a relatively more complicated system, it has been demonstrated in Ref. [55] that the exact dissociation curve of the N_2 molecule, using an active space of six electrons in 12 spin orbitals, is reproduced with satisfactory accuracy with the UCJ($L = 2$) ansatz when variationally optimized (classically). While it remains to be verified, we are optimistic that, for general molecular systems, the N^2 scaling of L can be reduced and in certain cases even excised. For illustrative purposes, the CNOT count for a given system size N with NOUCJ($L = 1$) is multiple orders of magnitude smaller than that from the Takagi-SVD decomposed NOUCC approach. For example, using two radical sites, 100 spin orbitals, and the NOUCC(2) routine assuming the 0.04 prefactor for L, it requires 6.3×10^7 CNOT gates, while the $L = 1$ NOUCJ approach requires only 1.3×10^5 gates. Clearly, this ansatz is a promising avenue forward and it will be investigated in future work.

In summary, our novel NOQE algorithm efficiently utilizes a quantum device to compute matrix elements of the Hamiltonian and the overlap involving nonorthogonal reference states (where we consider ansätze of the UCC and UCJ form). For a fixed number of reference states involved in the Hamiltonian diagonalization, the total number of CNOT and R_z gates required scales as $\mathcal{O}(N^2L)$ (assuming a first-order Trotter-Suzuki decomposition). The total gate cost per shot is summarized in Table VI. In order to resolve each element within some ϵ_{elem}, where we assume that the minimum matrix-element error threshold $\min(\epsilon_{\text{elem}})$ is used for all IJ pairs, we need to run the algorithm $\mathcal{O}(1/\epsilon_{\text{elem}}^2)$ times for each IJ element. With the UCJ($L = 1$) ansatz, the number of these gates will scale quadratically with the number of spin orbitals, while for Takagi- or SVD-decomposed UCC amplitudes, the counts will scale quartically.

TABLE VI. The asymptotic scaling of the number of CNOT and R_z gates as a function of the spin orbitals (N), the NO reference states (M), the Trotter-Suzuki decomposition order (k), and the Takagi-decomposition threshold (L) for a single shot of the NOQE circuit.

	CNOT and R_z gate complexity
CSWAP	$\mathcal{O}(N)$
$e^{\hat{\tau}}$	$\mathcal{O}(kN^2L)$
$\hat{\mathcal{U}}_{I\to 1}$	$\mathcal{O}(N^2)$
All H_{IJ} $(I \neq J)$	$\mathcal{O}(M^2kN^2L)$

B. Effects of noise and mitigation costs

While the primary purpose of the current work is to introduce the NOQE method and provide benchmark calculations demonstrating its potential with full unitary calculations, it is important to recognize that in near-term non-fault-tolerant implementations, the ansatz preparation circuits may be affected by stochastic device noise and by coherent noise from imperfect control of quantum gates. Noise mitigation techniques such as zero-noise extrapolation [109,110], virtual distillation [111,112], and randomized compilation [113,114] can mitigate the impact of noise, at the cost of requiring more circuit repetitions [115]. Readout errors may be addressable with classical postprocessing methods and thus have less impact on the quantum resources [116]. In addition, the underlying sampling noise associated with measurement of the Hamiltonian and overlap matrix elements, which will be present even in the fault-tolerant regime, will affect the precision of the resulting energies. The number of circuit repetitions required to reduce this sampling noise to achieve a specific precision will affect the overall scaling of the algorithm. Specifically, since the matrix elements are evaluated by a modified Hadamard test, where the output is measured by the result of a single-qubit measurement, each matrix element requires $\mathcal{O}(1/\epsilon_{\text{elem}}^2)$ repetitions of the circuit to resolve the value of the element within ϵ_{elem}. However, there is a nontrivial relationship between ϵ_{elem} and the desired error in the resulting eigenvalues ϵ for the generalized eigenvalue problem. Under specific assumptions, the bound on the number of circuit repetitions needed to resolve an eigenvalue can be computed and the resulting bound for these cases is discussed in Sec. S4C of the Supplemental Material [68]. We note furthermore that in a fault-tolerant implementation, the use of amplitude-amplification techniques [117] could reduce the dependence on ϵ_{elem} from $1/\epsilon_{\text{elem}}^2$ to $1/\epsilon_{\text{elem}}$.

VI. DISCUSSION

In this work, we present a nonorthogonal quantum eigensolver (NOQE) that provides a novel electronic structure method for computing low-lying eigenstates of strongly correlated molecular systems. The NOQE method produces multireference wave functions in which classically determined unitary coupled-cluster operators add dynamic correlation to each reference state. The set of correlated reference states, in which the Hamiltonian is diagonalized, is not constrained to be orthogonal. Our analysis shows that correlating nonorthogonal reference states with a cluster operator captures a significant portion of the exact wave function in a highly compact manner and, furthermore, that evaluation of the resulting energies is possible to compute at polynomial cost with a quantum computer. This is in stark contrast to the exponentially scaling number of resources required to implement such an algorithm on a classical computer. Thus a nonorthogonal multireference eigensolver is possible to implement in a scalable manner only on a quantum computer. NOQE provides a flexible, compact, and rigorous description of both strong and dynamic electronic correlations, making it an attractive method for the calculation of electronic states of a wide range of molecular systems.

The design principle behind NOQE is that the dynamically correlated UHF basis states are still each "single-reference" states, and that the subsequent CI part of the calculation (i.e., solving the generalized eigenvalue equation) recovers the correlation energy due to the multireference character. If the correlated reference states, before the CI, were to incorporate static correlations (i.e., were not strictly single-reference states), there would be diminishing returns, if any, from doing the CI part. Consider H_2 as a limiting example. CCSD with a UHF reference yields the exact wave function even beyond the CF point. In the context of NOQE, if the two UHF states (see top panel of Fig. 3) were correlated using t amplitudes from CCSD, the resulting correlated basis states would be identical and equal to the exact FCI wave function. Evaluating the Hamiltonian and overlap matrices in this basis would then be redundant and no excited-state information would result upon solving the generalized eigenvalue problem. Thus, for NOQE, the optimal correlators for each UHF state are those that provide an adequate but not necessarily exact description of electron correlation, i.e., those that accurately describe weak (dynamic) correlations while remaining single reference in nature. Hence, in this work we choose to use (scaled) MP2 amplitudes.

Concerning the amplitude scaling, it is well known that no universally optimal scaling factor exists. Practical ways forward, within the context of NOQE, include the empirical determination of optimal scaling factors on a wide variety of test sets. As mentioned above, forthcoming work in our group involves examining other nonempirical ways to dynamically correlate the NO single-reference states. Finally, leveraging the variationality of NOQE, it is possible to scan the scaling factor value for a given system to find an optimal value that leads to the lowest NOQE energy.

As has also been the case for classical NOCI calculations, the number of NO reference states in the NOQE approach still grows exponentially with the number of radical sites involved in the strong static correlation. However, this is a formal scaling that in practice is neither problematic nor relevant to most systems of chemical interest, since the number of radical sites typically does not reach large values for molecular systems (especially naturally occurring ones). In fact, there is a myriad of molecular systems of great chemical interest that only require a relatively small number of strongly correlated sites ($d < 8$), which NOQE is well suited to tackle, given appropriate quantum hardware. Such systems include dicopper subunits in metalloenzymes [118,119], n-carbenes or long polyacenes that possess di- and polyradical character [120], reduced states of metal complexes involving redox noninnocent ligands [4,121,122], and systems ranging from small transition-metal compounds to the OEC (four transition-metal sites), as mentioned in Sec. I, and iron-sulfur clusters (2–8 Fe atoms) [123–125].

A. Comparison with other quantum methods

In the context of previous quantum algorithms, NOQE possesses significant advantages over conventional variational quantum eigensolvers, for which a quantum device measures the energy while a classical device computes gradients and updates variational parameters for a given unitary ansatz. This results in a high measurement overhead from the input to the gradient and variational steps, both of which are absent in NOQE, while the need to compute gradients can result in getting trapped in the so-called "barren-plateau" parameter regions where the gradients become exponentially small as the problem size grows. Instead, the NOQE approach benefits from using a quantum processor to compute both matrix elements of the Hamiltonian and the set of overlap-matrix elements between dynamically correlated nonorthogonal states in parallel, at a low-order polynomial cost for a fixed number of radical sites.

The NOQE algorithm also allows simultaneous calculation of both ground and excited electronic eigenstates of the molecular Hamiltonian within the Born-Oppenheimer description (i.e., for fixed nuclear positions). In particular, our analysis of H_4 with the NOUCC(2) ansatz shows that the algorithm can efficiently compute the relative ordering and energy gaps of a select number of low-lying eigenstates in a single calculation without incurring additional measurement overhead, whereas the conventional VQE focuses on optimizing the ground state alone. While

excited-state estimates can in principle be obtained from a quantum subspace expansion (QSE) based on a single VQE ground state [126], we expect that the use by NOQE of multiple nonorthogonal reference states will enable a more flexible and compact description of strongly correlated states. We also note that NOQE amplitudes would provide a compact and high-quality guess for FCI eigenstates for use in fault-tolerant (i.e., non-near-term) algorithms such as quantum phase estimation (QPE) for estimating eigenvalues. The large improvement in fidelity over a single Slater Hartree-Fock reference is promising and efficient on a quantum computer but needs to be investigated further to show the overall cost-benefit analysis of this more involved state-preparation technique for QPE. It would be interesting here to compare the overall cost with that using classically determined NOCI amplitudes, which when combined with efficient preparation of multideterminant wave functions [127] would similarly provide a polynomially scaling alternative but one with reduced prefactors compared to NOQE.

Another major computational advantage of NOQE over the conventional variational approach embodied by the VQE is that our "one-shot" method, built on a multireference set of configuration interaction states, focuses on a chemistry-specific ansatz with significant input from classical quantum chemistry. This results in a very high-quality set of nonorthogonal reference states that do not require iterative parameter optimization on a quantum device. Instead, the expressivity of the output solution is provided by the multireference construction. The result is a dramatic reduction in both the gate complexity and the total number of measurements required to extract molecular energies or energy differences from running the algorithm on quantum devices. Furthermore, NOQE completely avoids the issues associated with possibly encountering a large number of nonglobal minima in the energy landscape when performing variational optimization or getting trapped on barren plateaus where the gradient nearly vanishes. These issues complicate the black-box use of the VQE and are particularly problematic for strongly correlated systems such as square H_4. We note that the variational step of the VQE does appear to provide some intrinsic error mitigation via the updating of circuit parameters in the classical optimization step, which is not present in NOQE. Instead, for the NOQE algorithm as for other nonvariational quantum algorithms, error mitigation on NISQ devices can be implemented by using the techniques of randomized compiling [113,114] or by methods based on virtual distillation [128,129].

From the perspective of seeking energies and wave functions for strongly correlated systems, the use of classically inspired ansätze, i.e., electronic wave-function forms that can be motivated and justified by chemical or physical insights, is an advantageous feature. Furthermore, the maturity of wave-function-based techniques for electronic structure calculations in classical quantum chemistry provides a well-paved roadmap for future improvements in NOQE. In this work, we focus primarily on using amplitudes from second-order perturbation theory within a UCCD-like ansatz, which are then decomposed to readily prepare relatively low-depth quantum circuits. As shown here for the examples of H_2 and H_4, this choice already leads to encouraging levels of accuracy, although achieving the goal of chemical accuracy in one shot (i.e., within 1.6 mHa of the exact values) requires amplitude-scaling procedures. We expect that there are other *ab initio* options for improving the ansatz states, beyond uniform or spin-component scaling, that do not dramatically increase the classical cost for preparing the ansatz states. Options include using amplitudes from CCSD [57] or from energy-gap-dependent regularized MP2 [130], as well as orbitals from methods other than Hartree-Fock [131,132]. Additionally, in this work, we take preliminary steps to explore the benefit of adding classically optimized Jastrow correlators to the UHF states, building a NOUCJ ansatz for NOQE, which appears to enable a reduction in the cost of quantum circuits for comparable accuracy for the H_2 system. In future work, we shall explore the performance of the classically variationally optimized NOUCJ ansatz for NOQE calculations of larger systems.

B. Comparison with classical methods

A few comments are in order to clarify the advantage of our quantum NOQE methods versus classical approaches. We note that classical projected coupled-cluster methods with truncated cluster operators also show formal polynomial scaling in the number of spin orbitals N. Indeed, the electronic ground states of the small H_2 and H_4 examples presented in this work can be exactly evaluated with polynomially scaling variants such as CCSD and CCSDTQ, respectively, acting on a single-reference Hartree-Fock determinant. However, excitations of order up to the number of radical sites d must be included in the cluster operator in order to exactly model an arbitrary strongly correlated system with CC, resulting in a classical computational cost that scales as $\mathcal{O}(N^{d+4})$. This approach would therefore be infeasible for larger systems such as dimetal complexes, where d is quite large. In practice, CC methods of higher order than CCSDTQ are seldom employed and almost never beyond rather small basis sets [133,134], restricting the practical utility of such classical methods to $d \leq 4$. Even CCSDTQ requires a very large amount of resources for systems as small as benzene in the cc-pVDZ basis [135]. Therefore, a multireference approach involving electron correlations between different radical sites is essential. The resource-estimate analysis in this work suggests that implementation of the polynomial scaling NOQE algorithm on quantum computers could be feasible for strongly correlated dimetallic species in the longer term.

The classical analog to NOQE would be variational NOCI-CC, which is intractable on classical computers. A related more approximate model is variational NOCI-MP2, i.e., NOCI with addition of MP2 correlations to the single-reference states, with all many-electron matrix elements rigorously evaluated. In this method, the calculation of matrix elements of the Hamiltonian and overlap between dynamically correlated nonorthogonal single-reference states also results in an intractably large number of terms. To avoid this, a viable NOCI-MP2 algorithm on classical computers [136] must make a potentially uncontrolled additional approximation: namely, to truncate the matrix elements at first or second order in the fluctuation potential for each many-electron basis state. However, this computationally viable NOCI-MP2 approach is no longer variational, unlike NOQE.

Other related classical analogs that target multireference systems include the complete active space second-order perturbation theory (CASPT2 [46,47]) and the closely related "N-electron valence space second-order perturbation theory" (NEVPT2 [48]) approaches, where exact diagonalization is performed within a predefined "active space" of a few electrons and orbitals assumed to be relevant for static correlation, followed by a perturbative treatment of dynamic correlation. This has obvious parallels with NOQE using exact diagonalization within a nonorthogonal basis for modeling strong correlation, with the unitary coupled-cluster operator, utilizing perturbative amplitudes in the NOUCC(2) implementation, accounting for dynamic correlation. While both CASPT2 or NEVPT2 and NOQE require an exponentially growing number of states (with respect to the number of radical sites) in the exact diagonalization step, the latter scales with a relatively softer exponential. Specifically, for the general case with d radical sites, η_α up spins and η_β down spins (where $\eta_\alpha + \eta_\beta < d$ and $m_s = \eta_\alpha - \eta_\beta$), the subspace for exact diagonalization in CASPT2 and NEVPT2 has a size M_{CAS},

$$M_{\mathrm{CAS}} = \frac{(d!)^2}{\eta_\alpha!\eta_\beta!(d-\eta_\alpha)!(d-\eta_\beta)!}, \tag{42}$$

which, as mentioned above, is much larger than the corresponding NOQE diagonalization subspace given by Eq. (27). In particular, for the case of $\eta_\alpha = \eta_\beta = d/2$, $M_{\mathrm{CAS}} = M_{\mathrm{NOQE}}^2$. The reduction in subspace size for NOQE is due to the fact that the use of nonorthogonal reference states allows for a more compact representation of the multireference wave function required for describing strong correlation. Furthermore, CASPT2 or NEVPT2 usually entails a self-consistent field (CASSCF [40]) stage, in which the M_{CAS} dimensional CAS wave function is iteratively optimized through repeated diagonalization and orbital rotations. In contrast, NOQE does not require any such optimization and is "one-shot" by construction. This leads to further computational efficiency compared to the classical CAS methods. We also note that the ground-state NOQE method is bounded from below by the FCI ground-state energy, which is not guaranteed to be the case for CASPT2 or NEVPT2. Indeed, while dynamic correlation in NOQE is evaluated through perturbative amplitudes, the use of the UCC formalism and diagonalization of the Hamiltonian within the subspace spanned by NO states enables NOQE to be more robust against failures sometimes encountered in purely perturbative classical theories [137–139]. In particular, the diagonal elements of the Hamiltonian in NOQE are correct to the third order in perturbation theory, indicating that NOQE goes beyond classical second-order perturbation theories for dynamic correlation outside the exact diagonalization subspace.

Finally, there is another very important point in which NOQE provides a significant advantage over classical algorithms in the case of multireference systems. This is that our hybrid quantum-classical NOQE implementation possesses long-sought-after properties of approximate methods to solve the electronic structure problem for ground and excited states. It is a basic tenet of quantum chemistry that such methods are necessarily based on approximate models, given the general infeasibility of finding the exact wave function for arbitrary chemical systems. Today's classical quantum chemistry methods are typically not both variational and size-extensive (the exceptions are the quite inaccurate mean-field HF or CIS approach and the completely intractable exact full CI model). Indeed, it has been argued that these properties are mutually exclusive [140]. For example, coupled-cluster algorithms rely on subspace projections to solve for the cluster amplitudes, while popular multireference approaches (e.g., CASPT2 and NEVPT2) rely on second-order perturbation theory—both of these types of models are not variational. Furthermore, CI methods (which also form the basis of QSE approaches) and even multireference generalizations of this are not size extensive. In this context, NOQE can be viewed as an approximate model for quantum chemistry of greater formal sophistication than all feasible and accurate classical approaches, in the sense that it is both variational *and* size extensive (given an appropriate choice of active spaces). UCC also shares these properties but NOQE can, in addition, treat strong and weak correlations in ground and excited states.

From the perspective of quantum chemistry, this appears to be a new type of practical quantum advantage in the sense that the NOQE model possesses a combination of desirable properties only attainable at present via a quantum algorithm. Indeed, it is unclear whether other approximate classical models with these desirable properties can even be developed in the future. This is distinct from a run-time quantum advantage based on asymptotic scaling of the algorithm with system size. While the time complexity of NOQE does also show polynomial scaling with the number of spin orbitals and comparison with alternative

multireference approaches such as CASPT2 and NEVPT2 shows a clear advantage for NOQE in terms of scaling with the number of radical sites, we believe that the combination of both variational character and size extensivity may constitute the most important quantum advantage of NOQE.

VII. CONCLUSIONS

In summary, the NOQE method presented in this work is a promising quantum electronic structure algorithm that excels at the accurate computation of energy gaps between low-lying eigenstates of a strongly correlated molecular system over a wide range of internuclear distances, allowing the construction of potential-energy surfaces for both ground and excited states. NOQE aims to systematically capture both static and dynamic correlation in a manner that is infeasible within a completely classical algorithm, whereas the quantum computer requires only a polynomial gate depth for a fixed number of radical sites. The method avoids the difficulties of variational optimization on quantum processors and instead takes advantage of carefully designed classical ansätze. We expect that the method will complement existing approaches for treating the ground states of strongly correlated systems when implemented on quantum computers in the fault-tolerant regime. The initial benchmark results presented here for H_2 and H_4 are encouraging. Future work will focus on performing NOQE calculations on currently available noisy intermediate-scale quantum devices, analyzing the effects of noise on these, investigating more sophisticated single-reference ansatz forms to employ in the NOQE multireference ansatz, and benchmarking the method for larger systems with more complex electronic structures.

ACKNOWLEDGMENTS

U.B., O.L., D.H., M.H.G., and K.B.W. were supported by the National Science Foundation (NSF) Quantum Leap Challenge Institutes (QLCI) program through Grant No. OMA-2016245. Early stages of this work were supported by the U.S. Department of Energy, Office of Science, Office of Advanced Scientific Computing Research, Quantum Algorithm Teams Program, under Contract No. DE-AC02-05CH11231 (U.B., W.H., and K.B.W.). J.S. acknowledges funding from the National Institute of General Medical Sciences of the National Institutes of Health under Award No. F32GM142231. T.F.S. is a Quantum Postdoctoral Fellow at the Simons Institute for the Theory of Computing, supported by the U.S. Department of Energy, Office of Science, National Quantum Information Science Research Centers, Quantum Systems Accelerator. We thank Hang Ren and Wendy Billings for helpful discussions and comments.

[1] B. O'Gorman, S. Irani, J. Whitfield, and B. Fefferman, Electronic structure in a fixed basis is QMA-complete, arXiv preprint arXiv:2103.08215 (2021).
[2] S. F. Boys and N. C. Handy, A calculation for the energies and wavefunctions for states of neon with full electronic correlation accuracy, Proc. R. Soc. Lond. A **310**, 63 (1969).
[3] D. W. Small and M. Head-Gordon, Post-modern valence bond theory for strongly correlated electron spins, Phys. Chem. Chem. Phys. **13**, 19285 (2011).
[4] J. Shee, M. Loipersberger, D. Hait, J. Lee, and M. Head-Gordon, Revealing the nature of electron correlation in transition metal complexes with symmetry breaking and chemical intuition, J. Chem. Phys. **154**, 194109 (2021).
[5] M. Imada, A. Fujimori, and Y. Tokura, Metal-insulator transitions, Rev. Mod. Phys. **70**, 1039 (1998).
[6] R. J. Witzke, D. Hait, K. Chakarawet, M. Head-Gordon, and T. D. Tilley, Bimetallic mechanism for alkyne cyclotrimerization with a two-coordinate Fe precatalyst, ACS Catal. **10**, 7800 (2020).
[7] C. A. Gould, K. R. McClain, D. Reta, J. G. C. Kragskow, D. A. Marchiori, E. Lachman, E.-S. Choi, J. G. Analytis, R. D. Britt, N. F. Chilton, B. G. Harvey, and J. R. Long, Ultrahard magnetism from mixed-valence dilanthanide complexes with metal-metal bonding, Science **375**, 198 (2022).
[8] M. Askerka, G. W. Brudvig, and V. S. Batista, The O_2-evolving complex of photosystem II: Recent insights from quantum mechanics/molecular mechanics (QM/MM), extended x-ray absorption fine structure (EXAFS), and femtosecond x-ray crystallography data, Acc. Chem. Res. **50**, 41 (2017).
[9] Y. Umena, K. Kawakami, J.-R. Shen, and N. Kamiya, Crystal structure of oxygen-evolving photosystem II at a resolution of 1.9 Å, Nature **473**, 55 (2011).
[10] J. Raymond and R. E. Blankenship, The origin of the oxygen-evolving complex, Coord. Chem. Rev. **252**, 377 (2008).
[11] A. Aspuru-Guzik, A. D. Dutoi, P. J. Love, and M. Head-Gordon, Simulated quantum computation of molecular energies, Science **309**, 1704 (2005).
[12] S. E. Smart and D. A. Mazziotti, Quantum Solver of Contracted Eigenvalue Equations for Scalable Molecular Simulations on Quantum Computing Devices, Phys. Rev. Lett. **126**, 070504 (2021).
[13] S. E. Smart and D. A. Mazziotti, Many-fermion simulation from the contracted quantum eigensolver without fermionic encoding of the wave function, Phys. Rev. A **105**, 062424 (2022).
[14] S. E. Smart, J.-N. Boyn, and D. A. Mazziotti, Resolving correlated states of benzyne with an error-mitigated contracted quantum eigensolver, Phys. Rev. A **105**, 022405 (2022).
[15] A. Peruzzo, J. McClean, P. Shadbolt, M.-H. Yung, X.-Q. Zhou, P. J. Love, A. Aspuru-Guzik, and J. L. O'Brien, A variational eigenvalue solver on a photonic quantum processor, Nat. Commun. **5**, 1 (2014).
[16] J. R. McClean, J. Romero, R. Babbush, and A. Aspuru-Guzik, The theory of variational hybrid quantum-classical algorithms, New J. Phys **18**, 023023 (2016).

[17] A. G. Taube and R. J. Bartlett, New perspectives on unitary coupled-cluster theory, Int. J. Quantum Chem. **106**, 3393 (2006).

[18] Google AI Quantum and Collaborators, Hartree-Fock on a superconducting qubit quantum computer, Science **369**, 1084 (2020).

[19] T. E. O'Brien *et al.*, Purification-based quantum error mitigation of pair-correlated electron simulations, arXiv:2210.10799 [quant-ph] (2022).

[20] J. Lee, W. J. Huggins, M. Head-Gordon, and K. B. Whaley, Generalized unitary coupled cluster wave functions for quantum computation, J. Chem. Theory Comput. **15**, 311 (2019).

[21] J. R. McClean, S. Boixo, V. N. Smelyanskiy, R. Babbush, and H. Neven, Barren plateaus in quantum neural network training landscapes, Nat. Commun. **9**, 1 (2018).

[22] A. Uvarov, J. D. Biamonte, and D. Yudin, Variational quantum eigensolver for frustrated quantum systems, Phys. Rev. B **102**, 075104 (2020).

[23] S. Wang, E. Fontana, M. Cerezo, K. Sharma, A. Sone, L. Cincio, and P. J. Coles, Noise-induced barren plateaus in variational quantum algorithms, Nat. Commun. **12**, 6961 (2021).

[24] A. Arrasmith, M. Cerezo, P. Czarnik, L. Cincio, and P. J. Coles, Effect of barren plateaus on gradient-free optimization, Quantum **5**, 558 (2021).

[25] E. R. Anschuetz and B. T. Kiani, Beyond barren plateaus: Quantum variational algorithms are swamped with traps, arXiv preprint arXiv:2205.05786 (2022).

[26] W. J. Huggins, J. Lee, U. Baek, B. O'Gorman, and K. B. Whaley, A non-orthogonal variational quantum eigensolver, New J. Phys. **22**, 073009 (2020).

[27] R. Broer and W. C. Nieuwpoort, Broken orbital-symmetry and the description of hole states in the tetrahedral $[CrO_4]^-$ anion. I. Introductory considerations and calculations on oxygen 1s hole states, Chem. Phys. **54**, 291 (1981).

[28] A. J. W. Thom and M. Head-Gordon, Hartree-Fock solutions as a quasidiabatic basis for nonorthogonal configuration interaction, J. Chem. Phys. **131**, 124113 (2009).

[29] E. J. Sundstrom and M. Head-Gordon, Non-orthogonal configuration interaction for the calculation of multielectron excited states, J. Chem. Phys. **140**, 114103 (2014).

[30] S. R. Yost and M. Head-Gordon, Size consistent formulations of the perturb-then-diagonalize Møller-Plesset perturbation theory correction to non-orthogonal configuration interaction, J. Chem. Phys. **145**, 054105 (2016).

[31] R. M. Parrish and P. L. McMahon, Quantum filter diagonalization: Quantum eigendecomposition without full quantum phase estimation, arXiv preprint arXiv:1909.08925 (2019).

[32] O. Kyriienko, Quantum inverse iteration algorithm for programmable quantum simulators, Npj Quantum Inf. **6**, 1 (2020).

[33] N. H. Stair, R. Huang, and F. A. Evangelista, A multireference quantum Krylov algorithm for strongly correlated electrons, J. Chem. Theory. Comput. **16**, 2236 (2020).

[34] K. Klymko, C. Mejuto-Zaera, S. J. Cotton, F. Wudarski, M. Urbanek, D. Hait, M. Head-Gordon, K. B. Whaley, J. Moussa, N. Wiebe, W. A. de Jong, and N. M. Tubman, Real-Time Evolution for Ultracompact Hamiltonian Eigenstates on Quantum Hardware, PRX Quantum **3**, 020323 (2022).

[35] J. Cohn, M. Motta, and R. M. Parrish, Quantum filter diagonalization with double-factorized Hamiltonians, arXiv preprint arXiv:2104.08957 (2021).

[36] A. Szabo and N. S. Ostlund, *Modern Quantum Chemistry: Introduction to Advanced Electronic Structure Theory* (Dover Publications, Inc., Mineola, New York, 1996), p. 286.

[37] J. D. Whitfield, P. J. Love, and A. Aspuru-Guzik, Computational complexity in electronic structure, Phys. Chem. Chem. Phys. **15**, 397 (2013).

[38] D. Cremer, Møller–Plesset perturbation theory: from small molecule methods to methods for thousands of atoms, Wiley Interdiscip. Rev. Comput. Mol. Sci. **1**, 509 (2011).

[39] R. J. Bartlett and M. Musiał, Coupled-cluster theory in quantum chemistry, Rev. Mod. Phys. **79**, 291 (2007).

[40] T. Helgaker, P. Jorgensen, and J. Olsen, *Molecular Electronic-Structure Theory* (John Wiley & Sons, Chichester, England, 2014).

[41] K. D. Vogiatzis, D. Ma, J. Olsen, L. Gagliardi, and W. A. De Jong, Pushing configuration-interaction to the limit: Towards massively parallel MCSCF calculations, J. Chem. Phys. **147**, 184111 (2017).

[42] N. M. Tubman, J. Lee, T. Y. Takeshita, M. Head-Gordon, and K. B. Whaley, A deterministic alternative to the full configuration interaction quantum Monte Carlo method, J. Chem. Phys. **145**, 044112 (2016).

[43] A. A. Holmes, N. M. Tubman, and C. J. Umrigar, Heat-bath configuration interaction: An efficient selected configuration interaction algorithm inspired by heat-bath sampling, J. Chem. Theory Comput. **12**, 3674 (2016).

[44] D. S. Levine, D. Hait, N. M. Tubman, S. Lehtola, K. B. Whaley, and M. Head-Gordon, Casscf with extremely large active spaces using the adaptive sampling configuration interaction method, J. Chem. Theory Comput. **16**, 2340 (2020).

[45] N. M. Tubman, C. D. Freeman, D. S. Levine, D. Hait, M. Head-Gordon, and K. B. Whaley, Modern approaches to exact diagonalization and selected configuration interaction with the adaptive sampling CI method, J. Chem. Theory Comput. **16**, 2139 (2020).

[46] K. Andersson, P. A. Malmqvist, B. O. Roos, A. J. Sadlej, and K. Wolinski, Second-order perturbation theory with a CASSCF reference function, J. Phys. Chem. **94**, 5483 (1990).

[47] K. Andersson, P.-Å. Malmqvist, and B. O. Roos, Second-order perturbation theory with a complete active space self-consistent field reference function, J. Chem. Phys. **96**, 1218 (1992).

[48] C. Angeli, R. Cimiraglia, S. Evangelisti, T. Leininger, and J.-P. Malrieu, Introduction of *n*-electron valence states for multireference perturbation theory, J. Chem. Phys. **114**, 10252 (2001).

[49] P. M. W. Gill, J. A. Pople, L. Radom, and R. H. Nobes, Why does unrestricted Møller-Plesset perturbation theory converge so slowly for spin-contaminated wave functions?, J. Chem. Phys. **89**, 7307 (1988).

[50] N. J. Mayhall, P. R. Horn, E. J. Sundstrom, and M. Head-Gordon, Spin-flip non-orthogonal configuration interaction: A variational and almost black-box method for describing strongly correlated molecules, Phys. Chem. Chem. Phys. **16**, 22694 (2014).

[51] I. Shavitt and R. J. Bartlett, *Many-Body Methods in Chemistry and Physics: MBPT and Coupled-Cluster Theory* (Cambridge University Press, Cambridge, England, 2009).

[52] M. Schütz, G. Hetzer, and H.-J. Werner, Low-order scaling local electron correlation methods. I. Linear scaling local MP2, J. Chem. Phys. **111**, 5691 (1999).

[53] C. Riplinger, P. Pinski, U. Becker, E. F. Valeev, and F. Neese, Sparse maps—a systematic infrastructure for reduced-scaling electronic structure methods. II. Linear scaling domain based pair natural orbital coupled cluster theory, J. Chem. Phys. **144**, 024109 (2016).

[54] J. E. Subotnik, A. Sodt, and M. Head-Gordon, A near linear-scaling smooth local coupled cluster algorithm for electronic structure, J. Chem. Phys. **125**, 074116 (2006).

[55] Y. Matsuzawa and Y. Kurashige, Jastrow-type decomposition in quantum chemistry for low-depth quantum circuits, J. Chem. Theory Comput. **16**, 944 (2020).

[56] S. McArdle, S. Endo, A. Aspuru-Guzik, S. C. Benjamin, and X. Yuan, Quantum computational chemistry, Rev. Mod. Phys. **92**, 015003 (2020).

[57] J. Romero, R. Babbush, J. R. McClean, C. Hempel, P. J. Love, and A. Aspuru-Guzik, Strategies for quantum computing molecular energies using the unitary coupled cluster ansatz, Quantum Sci. Technol. **4**, 014008 (2018).

[58] P. S. Epstein, The Stark effect from the point of view of Schroedinger's quantum theory, Phys. Rev. **28**, 695 (1926).

[59] R. K. Nesbet, Configuration interaction in orbital theories, Proc. R. Soc. Lond. A **230**, 312 (1955).

[60] C. Murray and E. R. Davidson, Different forms of perturbation theory for the calculation of the correlation energy, Int. J. Quantum Chem. **43**, 755 (1992).

[61] S. Grimme, Improved second-order Møller-Plesset perturbation theory by separate scaling of parallel-and antiparallel-spin pair correlation energies, J. Chem. Phys. **118**, 9095 (2003).

[62] Y. Jung, R. C. Lochan, A. D. Dutoi, and M. Head-Gordon, Scaled opposite-spin second order Møller-Plesset correlation energy: An economical electronic structure method, J. Chem. Phys. **121**, 9793 (2004).

[63] M. Motta, E. Ye, J. R. McClean, Z. Li, A. J. Minnich, R. Babbush, and G. K.-L. Chan, Low rank representations for quantum simulation of electronic structure, npj Quantum Inf. **7**, 1 (2021).

[64] N. C. Rubin, J. Lee, and R. Babbush, Compressing many-body fermion operators under unitary constraints, J. Chem. Theory Comput. **18**, 1480 (2022).

[65] E. P. Hoy and D. A. Mazziotti, Positive semidefinite tensor factorizations of the two-electron integral matrix for low-scaling *ab initio* electronic structure, J. Chem. Phys. **143**, 64103 (2015).

[66] B. Peng and K. Kowalski, Highly efficient and scalable compound decomposition of two-electron integral tensor and its application in coupled cluster calculations, J. Chem. Theory Comput. **13**, 4179 (2017).

[67] M. Motta, J. Shee, S. Zhang, and G. K.-L. Chan, Efficient ab initio auxiliary-field quantum Monte Carlo calculations in Gaussian bases via low-rank tensor decomposition, J. Chem. Theory Comput. **15**, 3510 (2019).

[68] See the Supplemental Material at http://link.aps.org/supplemental/10.1103/PRXQuantum.4.030307 for a brief introduction to quantum chemistry, along with additional data, details, and derivations.

[69] P. S. Bagus and B. I. Bennett, Singlet-triplet splittings as obtained from the $X\alpha$-scattered wave method: A theoretical analysis, Int. J. Quantum Chem. **9**, 143 (1975).

[70] C. A. Jimenez-Hoyos, T. M. Henderson, and G. E. Scuseria, Generalized Hartree-Fock description of molecular dissociation, J. Chem. Theory Comput. **7**, 2667 (2011).

[71] D. W. Small, E. J. Sundstrom, and M. Head-Gordon, A simple way to test for collinearity in spin symmetry broken wave functions: General theory and application to generalized Hartree-Fock, J. Chem. Phys. **142**, 094112 (2015).

[72] B. P. Pritchard, D. Altarawy, B. Didier, T. D. Gibson, and T. L. Windus, New basis set exchange: An open, up-to-date resource for the molecular sciences community, J. Chem. Inf. Model. **59**, 4814 (2019).

[73] R. Bauernschmitt and R. Ahlrichs, Stability analysis for solutions of the closed shell Kohn-Sham equation, J. Chem. Phys. **104**, 9047 (1996).

[74] J. Čížek and J. Paldus, Stability conditions for the solutions of the Hartree-Fock equations for atomic and molecular systems. application to the pi-electron model of cyclic polyenes, J. Chem. Phys. **47**, 3976 (1967).

[75] R. Seeger and J. A. Pople, Self-consistent molecular orbital methods. XVIII. Constraints and stability in Hartree-Fock theory, J. Chem. Phys. **66**, 3045 (1977).

[76] R. Mathias and C.-K. Li, The definite generalized eigenvalue problem: A new perturbation theory, (2004).

[77] G. W. Stewart, Perturbation bounds for the definite generalized eigenvalue problem, Linear Algebra Appl. **23**, 69 (1979).

[78] A. M. Childs, Y. Su, M. C. Tran, N. Wiebe, and S. Zhu, Theory of Trotter Error with Commutator Scaling, Phys. Rev. X **11**, 011020 (2021).

[79] W. Magnus, On the exponential solution of differential equations for a linear operator, Commun. Pure Appl. Math. **7**, 649 (1954).

[80] I. D. Kivlichan, J. McClean, N. Wiebe, C. Gidney, A. Aspuru-Guzik, G. K.-L. Chan, and R. Babbush, Quantum Simulation of Electronic Structure with Linear Depth and Connectivity, Phys. Rev. Lett. **120**, 110501 (2018).

[81] J. D. Whitfield, J. Biamonte, and A. Aspuru-Guzik, Simulation of electronic structure Hamiltonians using quantum computers, Mol. Phys. **109**, 735 (2011).

[82] M. B. Hastings, D. Wecker, B. Bauer, and M. Troyer, Improving quantum algorithms for quantum chemistry, Quantum Inf. Comput. **15**, 1 (2015).

[83] T. Kato, On the eigenfunctions of many-particle systems in quantum mechanics, Commun. Pure Appl. Math. **10**, 151 (1957).

[84] B. L. Hammond, W. A. Lester, and P. J. Reynolds, *Monte Carlo Methods in Ab Initio Quantum Chemistry* (World Scientific, Farrer Road, Singapore, 1994), Vol. 1.

[85] P. J. Reynolds, D. M. Ceperley, B. J. Alder, and W. A. Lester, Jr., Fixed-node quantum Monte Carlo for molecules, J. Chem. Phys. **77**, 5593 (1982).

[86] E. Neuscamman, Communication: A Jastrow factor coupled cluster theory for weak and strong electron correlation, J. Chem. Phys. **139**, 181101 (2013).

[87] E. Neuscamman, The Jastrow antisymmetric geminal power in Hilbert space: Theory, benchmarking, and application to a novel transition state, J. Chem. Phys. **139**, 194105 (2013).

[88] E. Neuscamman, Improved optimization for the cluster Jastrow antisymmetric geminal power and tests on triple-bond dissociations, J. Chem. Theory Comput. **12**, 3149 (2016).

[89] E. N. Epperly, L. Lin, and Y. Nakatsukasa, A theory of quantum subspace diagonalization, arXiv preprint arXiv:2110.07492 (2021).

[90] W. J. Huggins, J. R. McClean, N. C. Rubin, Z. Jiang, N. Wiebe, K. B. Whaley, and R. Babbush, Efficient and noise resilient measurements for quantum chemistry on near-term quantum computers, npj Quantum Inf. **7**, 1 (2021).

[91] J. R. McClean *et al.*, OpenFermion: The electronic structure package for quantum computers, Quantum Sci. Technol. **5**, 034014 (2020).

[92] Q. Sun *et al.*, Recent developments in the PySCF program package, J. Chem. Phys. **153**, 024109 (2020).

[93] E. Epifanovsky *et al.*, Software for the frontiers of quantum chemistry: An overview of developments in the Q-Chem 5 package, J. Chem. Phys. **155**, 084801 (2021).

[94] S. F. Boys, Construction of some molecular orbitals to be approximately invariant for changes from one molecule to another, Rev. Mod. Phys. **32**, 296 (1960).

[95] C. Edmiston and K. Ruedenberg, Localized atomic and molecular orbitals, Rev. Mod. Phys. **35**, 457 (1963).

[96] H. G. A. Burton and D. J. Wales, Energy landscapes for electronic structure, J. Chem. Theory Comput. **17**, 151 (2021).

[97] D. Hait and M. Head-Gordon, Excited state orbital optimization via minimizing the square of the gradient: General approach and application to singly and doubly excited states via density functional theory, J. Chem. Theory Comput. **16**, 1699 (2020).

[98] D. Hait and M. Head-Gordon, Orbital optimized density functional theory for electronic excited states, J. Chem. Phys. Lett. **12**, 4517 (2021).

[99] The CIRQ Developers, "CIRQ" (2019).

[100] C. A. Coulson and I. Fischer, XXXIV. Notes on the molecular orbital treatment of the hydrogen molecule, Philos. Mag. **40**, 386 (1949).

[101] D. Hait, A. Rettig, and M. Head-Gordon, Well-behaved versus ill-behaved density functionals for single bond dissociation: Separating success from disaster functional by functional for stretched H_2, J. Chem. Phys. **150**, 094115 (2019).

[102] N. Mardirossian and M. Head-Gordon, Thirty years of density functional theory in computational chemistry: An overview and extensive assessment of 200 density functionals, Mol. Phys. **115**, 2315 (2017).

[103] D. Hait, A. Rettig, and M. Head-Gordon, Beyond the Coulson-Fischer point: Characterizing single excitation CI and TDDFT for excited states in single bond dissociations, Phys. Chem. Chem. Phys. **21**, 21761 (2019).

[104] W. J. Hehre, R. F. Stewart, and J. A. Pople, Self-consistent molecular-orbital methods. I. Use of Gaussian expansions of Slater-type atomic orbitals, J. Chem. Phys. **51**, 2657 (1969).

[105] R. Ditchfield, W. J. Hehre, and J. A. Pople, Self-consistent molecular-orbital methods. IX. An extended Gaussian-type basis for molecular-orbital studies of organic molecules, J. Chem. Phys. **54**, 724 (1971).

[106] R. Krishnan, J. S. Binkley, R. Seeger, and J. A. Pople, Self-consistent molecular orbital methods. XX. A basis set for correlated wave functions, J. Chem. Phys. **72**, 650 (1980).

[107] B. O'Gorman, W. J. Huggins, E. G. Rieffel, and K. B. Whaley, Generalized swap networks for near-term quantum computing, arXiv preprint arXiv:1905.05118 (2019).

[108] A. Bocharov, M. Roetteler, and K. M. Svore, Efficient Synthesis of Universal Repeat-Until-Success Quantum Circuits, Phys. Rev. Lett. **114**, 080502 (2015).

[109] K. Temme, S. Bravyi, and J. M. Gambetta, Error Mitigation for Short-Depth Quantum Circuits, Phys. Rev. Lett. **119**, 180509 (2017).

[110] S. Endo, S. C. Benjamin, and Y. Li, Practical Quantum Error Mitigation for Near-Future Applications, Phys. Rev. X **8**, 031027 (2018).

[111] W. J. Huggins, S. McArdle, T. E. O'Brien, J. Lee, N. C. Rubin, S. Boixo, K. B. Whaley, R. Babbush, and J. R. McClean, Virtual Distillation for Quantum Error Mitigation, Phys. Rev. X **11**, 041036 (2021).

[112] B. Koczor, Exponential Error Suppression for Near-Term Quantum Devices, Phys. Rev. X. **11**, 031057 (2021).

[113] J. J. Wallman and J. Emerson, Noise tailoring for scalable quantum computation via randomized compiling, Phys. Rev. A **94**, 052325 (2016).

[114] A. Hashim, R. K. Naik, A. Morvan, J.-L. Ville, B. Mitchell, J. M. Kreikebaum, M. Davis, E. Smith, C. Iancu, K. P. O'Brien, I. Hincks, J. J. Wallman, J. Emerson, and I. Siddiqi, Randomized Compiling for Scalable Quantum Computing on a Noisy Superconducting Quantum Processor, Phys. Rev. X **11**, 041039 (2021).

[115] Z. Cai, R. Babbush, S. C. Benjamin, S. Endo, W. J. Huggins, Y. Li, J. R. McClean, and T. E. O'Brien, Quantum error mitigation, arXiv preprint arXiv:2210.00921 (2022).

[116] F. B. Maciejewski, Z. Zimborás, and M. Oszmaniec, Mitigation of readout noise in near-term quantum devices by classical post-processing based on detector tomography, Quantum **4**, 257 (2020).

[117] G. Brassard, P. Hoyer, M. Mosca, and A. Tapp, Quantum amplitude amplification and estimation, Contemp. Math. **305**, 53 (2002).

[118] B. F. Gherman and C. J. Cramer, Quantum chemical studies of molecules incorporating a $Cu_2O_2^{2+}$ core, Coord. Chem. Rev. **253**, 723 (2009).

[119] D. G. Liakos and F. Neese, Interplay of correlation and relativistic effects in correlated calculations on

transition-metal complexes: The $(Cu_2O_2)^{2+}$ core revisited, J. Chem. Theory Comput. **7**, 1511 (2011).
[120] Y. Yang, E. R. Davidson, and W. Yang, Nature of ground and electronic excited states of higher acenes, Proc. Natl. Acad. Sci. **113**, E5098 (2016).
[121] C. Römelt, J. Song, M. Tarrago, J. A. Rees, M. van Gastel, T. Weyhermüller, S. DeBeer, E. Bill, F. Neese, and S. Ye, Electronic structure of a formal Iron(0) porphyrin complex relevant to CO_2 reduction, Inorg. Chem. **56**, 4745 (2017).
[122] J. S. Derrick, M. Loipersberger, R. Chatterjee, D. A. Iovan, P. T. Smith, K. Chakarawet, J. Yano, J. R. Long, M. Head-Gordon, and C. J. Chang, Metal–ligand cooperativity via exchange coupling promotes iron-catalyzed electrochemical CO_2 reduction at low overpotentials, J. Am. Chem. Soc. **142**, 20489 (2020).
[123] S. Sharma, K. Sivalingam, F. Neese, and G. K. Chan, Low-energy spectrum of iron-sulfur clusters directly from many-particle quantum mechanics, Nat. Chem. **6**, 927 (2014).
[124] C. Mejuto-Zaera, D. Tzeli, D. Williams-Young, N. M. Tubman, M. Matoušek, J. Brabec, L. Veis, S. S. Xantheas, and W. A. de Jong, The effect of geometry, spin, and orbital optimization in achieving accurate, correlated results for iron-sulfur cubanes, J. Chem. Theory Comput. **18**, 687 (2022).
[125] Z. Li, J. Li, N. S. Dattani, C. J. Umrigar, and G. K.-L. Chan, The electronic complexity of the ground-state of the FeMo cofactor of nitrogenase as relevant to quantum simulations, J. Chem. Phys. **150**, 024302 (2019).
[126] J. R. McClean, M. E. Kimchi-Schwartz, J. Carter, and W. A. De Jong, Hybrid quantum-classical hierarchy for mitigation of decoherence and determination of excited states, Phys. Rev. A **95**, 042308 (2017).
[127] N. M. Tubman, C. Mejuto-Zaera, J. M. Epstein, D. Hait, D. S. Levine, W. Huggins, Z. Jiang, J. R. McClean, R. Babbush, and M. Head-Gordon *et al.*, Postponing the orthogonality catastrophe: Efficient state preparation for electronic structure simulations on quantum devices, arXiv preprint arXiv:1809.05523 (2018).
[128] W. J. Huggins, S. McArdle, T. E. O'Brien, J. Lee, N. C. Rubin, S. Boixo, K. B. Whaley, R. Babbush, and J. R. McClean, Virtual Distillation for Quantum Error Mitigation, Phys. Rev. X **11**, 041036 (2021).
[129] N. Yoshioka, H. Hakoshima, Y. Matsuzaki, Y. Tokunaga, Y. Suzuki, and S. Endo, Generalized Quantum Subspace Expansion, Phys. Rev. Lett. **129**, 020502 (2022).
[130] J. Shee, M. Loipersberger, A. Rettig, J. Lee, and M. Head-Gordon, Regularized second-order Møller-Plesset theory: A more accurate alternative to conventional MP2 for noncovalent interactions and transition metal thermochemistry for the same computational cost, J. Phys. Chem. Lett. **12**, 12084 (2021).
[131] L. W. Bertels, J. Lee, and M. Head-Gordon, Third-order Møller-Plesset perturbation theory made useful? choice of orbitals and scaling greatly improves accuracy for thermochemistry, kinetics, and intermolecular interactions, J. Phys. Chem. Lett. **10**, 4170 (2019).
[132] A. Rettig, D. Hait, L. W. Bertels, and M. Head-Gordon, Third-order Møller-Plesset theory made more useful? The role of density functional theory orbitals, J. Chem. Theory Comput. **16**, 7473 (2020).
[133] A. Karton, S. Daon, and J. M. L. Martin, W4-11: A high-confidence benchmark dataset for computational thermochemistry derived from first-principles W4 data, Chem. Phys. Lett. **510**, 165 (2011).
[134] D. Hait, N. M. Tubman, D. S. Levine, K. B. Whaley, and M. Head-Gordon, What levels of coupled cluster theory are appropriate for transition metal systems? A study using near-exact quantum chemical values for 3d transition metal binary compounds, J. Chem. Theory Comput. **15**, 5370 (2019).
[135] J. J. Eriksen *et al.*, The ground state electronic energy of benzene, J. Phys. Chem. Lett. **11**, 8922 (2020).
[136] S. R. Yost and M. Head-Gordon, Efficient implementation of NOCI-MP2 using the resolution of the identity approximation with application to charged dimers and long C—C bonds in ethane derivatives, J. Chem. Theory Comput. **14**, 4791 (2018).
[137] B. O. Roos and K. Andersson, Multiconfigurational perturbation theory with level shift—the Cr_2 potential revisited, Chem. Phys. Lett. **245**, 215 (1995).
[138] G. Ghigo, B. O. Roos, and P.-Å. Malmqvist, A modified definition of the zeroth-order Hamiltonian in multiconfigurational perturbation theory (CASPT2), Chem. Phys. Lett. **396**, 142 (2004).
[139] W. Kurlancheek and M. Head-Gordon, Violations of *N*-representability from spin-unrestricted orbitals in Møller-Plesset perturbation theory and related double-hybrid density functional theory, Mol. Phys. **107**, 1223 (2009).
[140] S. Hirata and I. Grabowski, On the mutual exclusion of variationality and size consistency, Thom H. Dunning, Jr. A Festschrift from Theoretical Chemistry Accounts, 267–275 (2015).